

1 Fundamental Oxidation Processes in the Remote  
2 Marine Atmosphere Investigated Using the NO-  
3 NO<sub>2</sub>-O<sub>3</sub> Photostationary State  
4

5 Simone T. Andersen<sup>1\*</sup>, Beth S. Nelson<sup>1</sup>, Katie A. Read<sup>1,2</sup>, Shalini Punjabi<sup>1,2</sup>, Luis Neves<sup>3</sup>,  
6 Matthew J. Rowlinson<sup>1</sup>, James Hopkins<sup>1,2</sup>, Tomás Sherwen<sup>1,2</sup>, Lisa K. Whalley<sup>2,4</sup>, James D.  
7 Lee<sup>1,2</sup>, and Lucy J. Carpenter<sup>1</sup>

8 <sup>1</sup>Wolfson Atmospheric Chemistry Laboratories (WACL), Department of Chemistry,  
9 University of York, Heslington, York, YO10 5DD, UK.

10 <sup>2</sup>National Centre for Atmospheric Science (NCAS), University of York, Heslington, York,  
11 YO10 5DD, UK.

12 <sup>3</sup>Instituto Nacional de Meteorologia e Geofísica, São Vicente (INMG), Mindelo, Cabo Verde.

13 <sup>4</sup>School of Chemistry, University of Leeds, Leeds, LS2 9JT

14 \*Corresponding author: [simone.andersen@york.ac.uk](mailto:simone.andersen@york.ac.uk)

15

# 1 Abstract

The photostationary state (PSS) equilibrium between NO and NO<sub>2</sub> is reached within minutes in the atmosphere and can be described by the PSS parameter,  $\phi$ . Deviations from expected values of  $\phi$  have previously been used to infer missing oxidants in diverse locations, from highly polluted regions to the extremely clean conditions observed in the remote marine boundary layer (MBL), and have been interpreted as missing understanding of fundamental photochemistry. Here, contrary to these previous observations, we observe good agreement between PSS-derived NO<sub>2</sub> ( $[\text{NO}_2]_{\text{PSS ext.}}$ )<sub>2</sub> calculated from measured NO, O<sub>3</sub>, and jNO<sub>2</sub> and photochemical box model predictions of peroxy radicals (RO<sub>2</sub> and HO<sub>2</sub>) ~~and measured NO, O<sub>3</sub>, and jNO<sub>2</sub>~~, and observed NO<sub>2</sub> ( $[\text{NO}_2]_{\text{Obs.}}$ ) in extremely clean air containing low levels of CO (< 90 ppbV) and VOCs. However, in clean air containing small amounts of aged pollution (CO > 100 ppbV), we observed higher levels of NO<sub>2</sub> than inferred from the PSS, with  $[\text{NO}_2]_{\text{Obs.}}/[\text{NO}_2]_{\text{PSS ext.}}$  of 1.12-1.68 (25<sup>th</sup>-75<sup>th</sup> percentile) implying underestimation of RO<sub>2</sub> radicals by 18.5-104 pptV ~~(25<sup>th</sup>-75<sup>th</sup> percentile) of missing RO<sub>2</sub> radicals~~. Potential NO<sub>2</sub> measurement artefacts have to be carefully considered when comparing PSS-derived NO<sub>2</sub> to observed NO<sub>2</sub>, but we show that the NO<sub>2</sub> artefact required to explain the deviation would have to be ~ 4 times greater than the maximum calculated from known interferences. If the additional missing RO<sub>2</sub> radicals inferred from the PSS convert NO to NO<sub>2</sub> with a reaction rate ~~have an ozone production efficiency~~ equivalent to that of methyl peroxy radicals (CH<sub>3</sub>O<sub>2</sub>), then the calculated net ozone production rate (NOPR, ppbV/h) including these additional oxidants is similar to the average change in O<sub>3</sub> ~~at~~ observed, within estimated uncertainties, once halogen oxide chemistry is accounted for. This implies that such additional peroxy radicals, cannot be excluded as ~~the~~ missing oxidant in clean marine air containing aged pollution, and that ~~measured and modelled RO<sub>2</sub> concentrations are~~ are both significantly underestimated under these conditions.

# 2 Introduction

Tropospheric NO, NO<sub>2</sub> and O<sub>3</sub> are rapidly interconverted during the day via reactions (1-3), where NO is oxidised by O<sub>3</sub> into NO<sub>2</sub>, which is then photolyzed into NO and O(<sup>3</sup>P), followed by a fast reaction of O(<sup>3</sup>P) with O<sub>2</sub> to return O<sub>3</sub>.





49 The photostationary state (PSS) equilibrium between NO and NO<sub>2</sub> is reached within  
 50 minutes (Leighton, 1961) if it is not impacted by fresh NO<sub>x</sub> emissions and if the photolysis rate  
 51 does not change quickly such as under rapidly changing cloud coverage (Mannschreck et al.,  
 52 2004). The photostationary state can be described by the Leighton ratio (Leighton, 1961) (eq.  
 53 I), where  $j\text{NO}_2$  is the photolysis rate of NO<sub>2</sub> and  $\phi$  is the PSS parameter.

54 
$$\phi = \frac{j\text{NO}_2[\text{NO}_2]}{k_1[\text{NO}][\text{O}_3]} \quad (\text{I})$$

55 Under ~~very polluted~~ conditions, where O<sub>3</sub> is the only oxidant converting NO to NO<sub>2</sub>,  
 56 such as during very low sunlight or very high NO mixing ratios  $\phi$  is equal to 1 and ~~the~~ NO<sub>2</sub> at  
 57 PSS can be estimated from the measured NO, O<sub>3</sub>, and  $j\text{NO}_2$  (eq. II).

58 
$$[\text{NO}_2]_{\text{PSS}} = \frac{k_1[\text{NO}][\text{O}_3]}{j\text{NO}_2} \quad (\text{II})$$

59 Deviations from  $\phi = 1$  suggest the presence of additional chemistry occurring (Calvert  
 60 and Stockwell, 1983), particularly the conversion of NO to NO<sub>2</sub> by reaction with an oxidant  
 61 other than O<sub>3</sub>, such as hydroperoxy radicals (HO<sub>2</sub>) and organic peroxy radicals (RO<sub>2</sub>) (reactions  
 62 4-5, where R represents any organic functional group) or with halogen oxides (IO, BrO;  
 63 reactions 6-7) in the marine atmosphere.



68 By including these additional NO oxidation reactions, the NO<sub>2</sub> concentration at PSS  
 69 can be estimated using equation (III). The photostationary state of NO/NO<sub>2</sub> can also be used to  
 70 estimate the sum of HO<sub>2</sub> and RO<sub>2</sub> (RO<sub>x</sub>) or the sum of BrO and IO (XO) in the atmosphere  
 71 using equation (IV) and (V) and assuming that  $k_4 = k_5$  and  $k_6 = k_7$ , respectively:

72 
$$[\text{NO}_2]_{\text{PSS ext.}} = \frac{(k_1[\text{O}_3] + k_4[\text{RO}_2] + k_5[\text{HO}_2] + k_6[\text{IO}] + k_7[\text{BrO}])[\text{NO}]}{j\text{NO}_2} \quad (\text{III})$$

$$73 \quad [\text{RO}_2] + [\text{HO}_2] = \frac{j\text{NO}_2[\text{NO}_2] - (k_1[\text{O}_3] + k_6[\text{IO}] + k_7[\text{BrO}])[\text{NO}]}{k_{4,5}[\text{NO}]} \quad (\text{IV})$$

$$74 \quad [\text{BrO}] + [\text{IO}] = \frac{j\text{NO}_2[\text{NO}_2] - (k_1[\text{O}_3] + k_4[\text{RO}_2] + k_5[\text{HO}_2])[\text{NO}]}{k_{6,7}[\text{NO}]} \quad (\text{V})$$

75 Previous studies reporting deviations in the PSS parameter to estimate RO<sub>x</sub>  
 76 concentrations in the atmosphere are summarised in Table 1, which compares [RO<sub>x</sub>]<sub>PSS</sub> against  
 77 measured and/or modelled [RO<sub>x</sub>]. Measurements of RO<sub>x</sub> are predominantly conducted using  
 78 chemical amplification, where each RO<sub>2</sub> and HO<sub>2</sub> molecule in ambient air leads to the  
 79 formation of several NO<sub>2</sub> molecules by chain reactions caused by the addition of high  
 80 concentrations of NO and CO (Cantrell et al., 1993b). The resultant NO<sub>2</sub> can be detected and  
 81 converted back to a RO<sub>x</sub> concentration by quantification of the chain length of the reactions  
 82 via calibration, typically using known concentrations of CH<sub>3</sub>O<sub>2</sub> or peroxyacetyl (CH<sub>3</sub>C(O)O<sub>2</sub>)  
 83 radicals (Cantrell et al., 1993b; Miyazaki et al., 2010; Wood and Charest, 2014). Since the basis  
 84 of the chemical amplification technique is detection of RO<sub>x</sub> radicals from their ability to oxidise  
 85 NO to NO<sub>2</sub> (reactions 4 and 5), which is also used to estimate RO<sub>x</sub> from the PSS, the RO<sub>x</sub>  
 86 concentrations determined from these methods would be expected to agree reasonably well.  
 87 However, PSS-derived RO<sub>x</sub> concentrations are generally higher than both measured values and  
 88 those calculated modelled from models and steady state equations-values in rural conditions  
 89 (Cantrell et al., 1997; Cantrell et al., 1993a; Ma et al., 2017; Mannschreck et al., 2004; Volz-  
 90 Thomas et al., 2003) with exceptions such as in the Pearl River Delta where PSS-derived and  
 91 measured RO<sub>x</sub> were comparable (Ma et al., 2017). During campaigns in relatively clean regions  
 92 with moderate influence from pollution (Amazon Basin and Arabian Peninsula), median PSS-  
 93 derived RO<sub>x</sub>/modelled RO<sub>x</sub> (both box and 3D)-levels ratios have been shown to be around 1,  
 94 albeit, with large variations in the data~~in good agreement with modelled RO<sub>x</sub>~~ (Tadic et al.,  
 95 2020; Trebs et al., 2012). In the remote marine boundary layer (MBL), PSS-derived RO<sub>x</sub> has  
 96 been observed to be 1.27 times higher than the measured RO<sub>x</sub> over the South Atlantic Ocean,  
 97 which itself~~however, the measured RO<sub>x</sub>~~ was approximately 4 times higher than box-modelled  
 98 (Hosaynali Beygi et al., 2011).

99 ~~The d~~Differences between measured, modelled, and PSS-derived RO<sub>x</sub> can be due to a  
 100 variety of reasons. RO<sub>x</sub> concentrations calculated by box models rely on comprehensive  
 101 constraint from co-measured trace gases and a reaction scheme which accurately represents the  
 102 most important photochemical processes. Incomplete characterization of ambient trace gases  
 103 and/or reaction schemes can therefore result in uncertain RO<sub>x</sub> predictions. Large deviations

104 (factor of ~ 3) between box modelled and measured RO<sub>x</sub> levels in a pine forest in the Rocky  
105 Mountains were attributed to a combination of a missing photolytic source of HO<sub>2</sub> at midday  
106 and a missing reaction forming RO<sub>2</sub> independently of sunlight in the model scheme (Wolfe et  
107 al., 2014). PSS-derived RO<sub>x</sub> can be significantly over- or underestimated if ~~the~~ PSS has not  
108 been established, for example due to rapidly changing photolysis rates or local sources of NO<sub>x</sub>  
109 (Mannschreck et al., 2004). Another reason for overestimation of PSS-derived RO<sub>x</sub> is NO<sub>2</sub>  
110 measurement artefacts (Bradshaw et al., 1999; Crawford et al., 1996), which results in  
111 overestimated NO<sub>2</sub> concentrations. These are common in chemiluminescence instruments and  
112 can be due to photolytic or thermal decomposition of HONO, peroxyacetyl nitrate (PAN), and  
113 other nitrate molecules in the atmosphere (Bradshaw et al., 1999; Gao et al., 1994; Parrish et  
114 al., 1990; Pollack et al., 2010; Reed et al., 2016; Ridley et al., 1988; Ryerson et al., 2000).

115 Measurements of RO<sub>x</sub> are also not without challenges due to effects from e.g. the high  
116 reactivity of RO<sub>x</sub>, humidity, non-linearity of the NO<sub>2</sub> detection, and formation of organic  
117 nitrates and nitrites. In the first chemical amplification instruments, NO<sub>2</sub> was detected by  
118 luminol chemiluminescence, which has a non-linear response to NO<sub>2</sub> resulting in the need for  
119 a multipoint calibration (Cantrell et al., 1997). However, more recent instruments use cavity  
120 ~~attenuated absorption~~ phase shift (CAPS) spectroscopy (Duncianu et al., 2020; Wood and  
121 Charest, 2014), laser induced fluorescence (LIF) (Sadanaga et al., 2004), or cavity ring-down  
122 spectroscopy (CRDS) (Liu and Zhang, 2014) for detection of NO<sub>2</sub>, all of which have been  
123 shown to have a linear response. Chemical amplifiers are usually only calibrated for one or two  
124 types of peroxy radicals. However, the chain length of each peroxy radical varies, resulting in  
125 a different amount of NO<sub>2</sub> production depending on the mixture of peroxy radicals present,  
126 which could lead to over/underestimations depending on the ambient mixture. Additionally,  
127 the chain length is significantly affected by humidity due to the increase in HO<sub>2</sub> wall loss on  
128 humidwet surfaces and to an enhanced termination rate of HO<sub>2</sub> by reaction with NO to give  
129 HNO<sub>3</sub>. HO<sub>2</sub> has been shown to form a complex with H<sub>2</sub>O (HO<sub>2</sub>·H<sub>2</sub>O), which reacts 4-8 times  
130 faster with NO, creating HNO<sub>3</sub>, at 50% relative humidity (RH) compared to under dry  
131 conditions (Butkovskaya et al., 2007; Butkovskaya et al., 2009; Duncianu et al., 2020). This  
132 leads to the measured chain length decreasing by a factor of two when going from dry  
133 conditions to 40% RH and by a factor of three at 70% RH (Duncianu et al., 2020; Mihele and  
134 Hastie, 1998). Finally, the chain length is impacted by the gas reagents (NO and CO). Peroxy  
135 radicals and alkoxy radicals (RO) can react with NO to create organic nitrates and nitrites,  
136 which terminates the chain reaction, preventing further radical propagation processes. This is

137 favoured by longer chain peroxy radicals, and at high NO concentrations. The formation yield  
138 of organic nitrates and nitrites differs from a few percent to up to ~23% depending on the nature  
139 of the R group present (Duncianu et al., 2020). The studies summarised in Table 1 using  
140 chemical amplification to measure total RO<sub>x</sub> have estimated the total uncertainty of the  
141 measurements to vary from 10-60% (1σ) with the most recent study estimating the highest  
142 uncertainty (Ma et al., 2017). ~~It is therefore important to determine the optimal concentrations~~  
143 ~~of reagent gas for each individual instrument as it could vary with what material has been used~~  
144 ~~in the reactor.~~

145 In the presence of sufficient levels of NO, additional ambient peroxy radicals not  
146 accounted for in photochemical models should lead to an underestimation of the simulated  
147 production rate of O<sub>3</sub>, which occurs via reactions (4) and (5) followed by photolysis of NO<sub>2</sub>.  
148 The production rate of O<sub>3</sub> (P(O<sub>3</sub>)) can be calculated using equation (VI):

$$149 \quad P(\text{O}_3) = k_4[\text{NO}][\text{RO}_2] + k_5[\text{NO}][\text{HO}_2] \quad (\text{VI})$$

150 Volz-Thomas et al. (2003) calculated O<sub>3</sub> production rates from PSS-derived and  
151 chemical amplification-measured RO<sub>x</sub> during the BERLIOZ campaign in Pabstthum,  
152 Germany, resulting in an average of ~ 20 ppbV h<sup>-1</sup> and ~ 2 ppbV h<sup>-1</sup> across the campaign,  
153 respectively. The large difference was credited to an unknown process that converts NO into  
154 NO<sub>2</sub> without causing additional O<sub>3</sub> production (Volz-Thomas et al., 2003). This is possible if  
155 NO is oxidised by an oxidant which also destroys O<sub>3</sub>, similarly to halogen atoms/halogen  
156 oxides. This hypothesis is consistent with observations by Parrish et al. at a mountain station  
157 in Colorado, where a missing oxidant of photolytic origin was identified (Parrish et al., 1986).  
158 It was shown that if the NO to NO<sub>2</sub> oxidation was completely due to RO<sub>x</sub>, the increased O<sub>3</sub>  
159 production would result in O<sub>3</sub> mixing-ratio levels significantly higher than measured, yet if the  
160 oxidant exhibited similar reaction mechanisms to IO, extremely high (70 pptV) mixing ratios  
161 of IO would be needed (Parrish et al., 1986). These IO levels are more than an order of  
162 magnitude higher than observations in the marine atmosphere (Inamdar et al., 2020; Mahajan  
163 et al., 2010; Prados-Roman et al., 2015; Read et al., 2008).

164 In regions where the net O<sub>3</sub> production rate (NOPR) is negligible or negative during the  
165 day due to very low NO levels, it is more relevant to compare the net ozone production rate  
166 (NOPR) to the observed change in [O<sub>3</sub>]. The chemical NOPR can be calculated as the  
167 difference between the photochemical processes producing and destroying O<sub>3</sub>:

$$168 \quad \text{NOPR} = \text{P}(\text{O}_3) - \text{L}(\text{O}_3) \quad (\text{VII})$$

169 where  $\text{P}(\text{O}_3)$  is determined using equation (VI) and the loss rate of  $\text{O}_3$  ( $\text{L}(\text{O}_3)$ ), is usually  
 170 determined from reactions (8-12). Additionally, halogens have previously been shown to cause  
 171 an  $\text{O}_3$  loss of  $0.23 \pm 0.05$  ppbV  $\text{h}^{-1}$  in the MBL (initiated by reaction 13) (Read et al., 2008),  
 172 which is in line with other studies suggesting that halogens can have a significant impact on  $\text{O}_3$   
 173 in marine environments (Saiz-Lopez et al., 2012; Sherwen et al., 2016; Vogt et al., 1999).



180 The actual rate of change of  $[\text{O}_3]$  within the planetary boundary layer is also impacted  
 181 by the physical processes of advection, deposition and entrainment, which complicates  
 182 comparisons with the NOPR. However, if these physical processes change only negligibly over  
 183 the course of a day, such as in marine well mixed air masses, their net influence can be deduced  
 184 from the net night time change in  $\text{O}_3$  (Ayers and Galbally, 1995; Ayers et al., 1992; Read et  
 185 al., 2008), allowing a calculation of the NOPR from observations. A comparison of the  
 186 observed and calculated NOPR gives an indication of whether production and loss rates of  $\text{O}_3$   
 187 from known processes are sufficient to explain the observed  $\text{O}_3$  tendencyphotochemical regime  
 188 (Read et al., 2008).

189 From the studies shown in Table 1, there is clearly widespread evidence of enhanced  
 190 PSS-derived  $\text{RO}_2$  compared to measurements and models, however, all methods to derive  $\text{RO}_x$   
 191 are not without challenges as described above. The large uncertainties associated with  $\text{RO}_x$   
 192 measurements, especially at high humidities where the chain length is significantly impacted  
 193 by enhanced wall loss and the production of  $\text{HNO}_3$ , suggest that measurements could be  
 194 underestimating  $\text{RO}_x$  in the atmosphere. Previous studies also find that the additional  
 195 conversion of  $\text{NO}$  to  $\text{NO}_2$  caused by the extra “ $\text{RO}_2$ ” should only produce minimal additional



196 O<sub>3</sub>, or at least lead to additional O<sub>3</sub> destruction, thus inferring an unknown missing oxidant  
197 which exhibits different chemical behaviour to peroxy radicals.

198 Up to 25% of methane removal occurs in the tropical MBL due to the high  
199 photochemical activity and humidity resulting in high OH radical concentrations (Bloss et al.,  
200 2005). Thus, it is crucially important to understand the fundamental oxidation processes, such  
201 as the NO<sub>x</sub>-O<sub>3</sub> cycle, occurring in this region. However, remote NO<sub>x</sub> measurements are rare  
202 due to the difficulty in measuring very low (pptV) mixing ratios. Most previous remote NO<sub>x</sub>  
203 measurements have taken place during short campaigns and do not give information on  
204 seasonal changes and long-term trends (Carsey et al., 1997; Jacob et al., 1996; Peterson and  
205 Honrath, 1999; Rhoads et al., 1997). Here, we investigate the photostationary state under clean  
206 marine conditions from three years of observations (2017-2020) at the Cape Verde  
207 Atmospheric Observatory (CVAO) in the tropical east Atlantic, representing a unique dataset  
208 to investigate NO<sub>x</sub>-O<sub>3</sub> chemistry in the remote MBL (Andersen et al., 2021; Carpenter et al.,  
209 2010; Lee et al., 2009). We also compare the chemical net O<sub>3</sub> production rate (NOPR)  
210 calculated from a box model with NOPR derived from the observed net O<sub>3</sub> rate of change, in  
211 order to evaluate the possibility of missing peroxy radicals in this remote environment.

212

## 213 3 Methods

### 214 3.1 Measurements

215 Year-round measurements of meteorological parameters and trace gases including NO,  
216 NO<sub>2</sub>, and C<sub>2</sub>-C<sub>8</sub> VOCs have been conducted at the CVAO (16° 51' N, 24° 52' W) since October  
217 2006. The CVAO is located on the north eastern coast of São Vicente, Cabo Verde. The air  
218 sampled predominantly comes from the northeast (see Figure 1) and has travelled over the  
219 Atlantic Ocean for multiple days since the last exposure to anthropogenic emissions, with the  
220 potential exception of ship emissions (Carpenter et al., 2010; Read et al., 2008). This makes it  
221 an ideal location to investigate fundamental photochemistry in an ultra-clean environment.

222 Wind speed (m/s), wind direction (°), temperature (°C), relative humidity (%),  
223 barometric pressure (mbar) and total solar radiation (W/m<sup>2</sup>) are measured at a height of 7.5 m  
224 using an automatic weather station from Campbell Scientific. NO and NO<sub>2</sub> have been measured  
225 using an ultra-high sensitivity NO chemiluminescence instrument, which measures NO<sub>2</sub> by  
226 photolytic conversion to NO, at the CVAO since 2006 (Lee et al., 2009). The technique and



227 data analysis have been described in detail elsewhere (Andersen et al., 2021). O<sub>3</sub> is measured  
228 using a Thermo Scientific 49i Ozone monitor as described in Read et al. (2008). Photolysis  
229 rates of a variety of species were measured in 2020 using a spectral radiometer (a 2-pi sr quartz  
230 diffuser coupled to an Ocean Optics QE65000 spectrometer via a 10 m fibre optic cable). Prior  
231 to 2020, photolysis rates are calculated in this study based on the correlation between the  
232 measured photolysis rates in 2020 and the total solar radiation, as described in the  
233 supplementary information. Average  $j\text{NO}_2$  and  $j\text{O}(^1\text{D})$  for different seasons are shown in Table  
234 2. VOCs are measured using a dual channel Agilent 7890A gas chromatograph coupled with a  
235 Flame Ionization Detector (GC-FID) and a MARKES Thermal Desorption Unit with an ozone  
236 precursor trap that is cooled to -30 °C (Read et al., 2009). Details of the calibration and  
237 uncertainties are given in the World Calibration Centre (WCC)-VOC audit report  
238 (Steinbrecher, 2019). Examples of the VOCs measured at the CVAO can be found in Table 2.  
239 Carbon monoxide (CO), and methane (CH<sub>4</sub>), are measured using a cavity ring-down  
240 spectrometer (CRDS), G2401 manufactured by Picarro Inc, following the Global Atmosphere  
241 Watch (GAW) recommended technique for long term remote measurements. The instrument  
242 is highly linear, has a precision of 1 ppbV and 0.3 ppbV over 10 minutes for CO and CH<sub>4</sub>  
243 respectively and no measurable drift (Zellweger et al., 2016; Zellweger et al., 2012).

244 Time series of NO, NO<sub>2</sub>, O<sub>3</sub>,  $j\text{NO}_2$ ,  $j\text{O}(^1\text{D})$ , temperature, CO, propene, benzene and  
245 CH<sub>4</sub> for July 2017 – June 2020 are shown in figures S4-S6. The specifics of each instrument  
246 and their respective measurements can be found in Table 2 and a full description of the CVAO  
247 site and associated measurements is given in Carpenter et al. (2010).

248

### 249 3.1.1 NO<sub>2</sub> Measurement Artefact

250 One of the drawbacks of measuring NO<sub>2</sub> by photolytic conversion to NO is it can be  
251 subject to artefacts. These could either be of a photolytic or thermal origin (Bradshaw et al.,  
252 1999; Gao et al., 1994; Parrish et al., 1990; Ridley et al., 1988; Ryerson et al., 2000). Photolytic  
253 artefacts occur when other compounds containing -NO, -NO<sub>2</sub>, or -NO<sub>3</sub> photolyse to form NO  
254 over a similar wavelength range as NO<sub>2</sub> and thereby produce an overestimate of NO<sub>2</sub> in the  
255 sample (Pollack et al., 2010). Thermal artefacts are caused by thermally labile compounds  
256 which decompose in photolytic converters when they heat up and release NO that is measured  
257 by the detector or NO<sub>2</sub> which is immediately photolytically converted to NO and then detected  
258 (Reed et al., 2016). Additional artefact can arise from compounds sticking to the converter and

259 creating an artefact when the converter is switched on. The ~~maximum~~ potential NO<sub>2</sub> artefact  
260 can be estimated using measured or modelled mixing ratios of a range of potential interfering  
261 compounds.

262 The photolytic contribution can be estimated based on the absorption cross section  
263 (ACS) of NO<sub>2</sub> and the potential interferents around the peak wavelength of the diodes used to  
264 convert NO<sub>2</sub> into NO (385 ± 5 nm). The ACS of NO<sub>2</sub> and some known interfering compounds  
265 over the wavelength range 380–390 nm are shown in Table 3. NO<sub>2</sub> and most of the interferents,  
266 with the exception of HONO, show relatively invariant ACSs across these wavelengths. When  
267 the ACSs of both NO<sub>2</sub> and the particular interferent are invariant over the spectral output of the  
268 diodes, the ratio at the peak wavelength is used to estimate the potential artefact. However,  
269 since the ACS of HONO varies significantly over the range, the HONO/NO<sub>2</sub> ACS ratio has  
270 been estimated assuming a Gaussian output of the diodes over the wavelengths. It is also  
271 important to take into account whether photolysis of the potential interferent produces NO<sub>2</sub> or  
272 NO. If NO is the product, then one converted molecule will be detected as two NO<sub>2</sub> molecules  
273 if the conversion efficiency of NO<sub>2</sub> is 50 %. If NO<sub>2</sub> is the product then it will be photolysed to  
274 NO with a lower conversion efficiency than NO<sub>2</sub> due to spending less time in the converter  
275 than ambient NO<sub>2</sub>. However, the conversion efficiency of NO<sub>2</sub> is used here (Table 3) to  
276 determine an upper limit of the contribution to the NO<sub>2</sub> artefact.~~the same efficiency as NO<sub>2</sub> in~~  
277 ~~the ambient air, however, if NO is the product then 1 converted molecule will be detected as 2~~  
278 ~~NO<sub>2</sub> molecules if the conversion efficiency of NO<sub>2</sub> is 50 %.~~ The investigated O<sub>o</sub>rganic nitrates  
279 (C<sub>2</sub>H<sub>5</sub>ONO<sub>2</sub>, CH<sub>3</sub>ONO<sub>2</sub>, *n*- and *i*-C<sub>3</sub>H<sub>7</sub>ONO<sub>2</sub>, 1- and 2-C<sub>4</sub>H<sub>9</sub>ONO<sub>2</sub>, CH<sub>3</sub>O<sub>2</sub>NO<sub>2</sub>, and  
280 CH<sub>3</sub>C(O)O<sub>2</sub>NO<sub>2</sub>), HNO<sub>3</sub>, and NO<sub>3</sub> do not photolyse at 385 nm and have therefore not been  
281 included in the evaluation of photolytic artefacts (Atkinson et al., 2004).

282 The main potential photolytic artefact for the CVAO NO<sub>2</sub> measurements is HONO.  
283 Measurements of HONO at the CVAO using a Long Path Absorption Photometer (LOPAP)  
284 show levels of up to ~ 5 pptV (Reed et al., 2017), indicating an NO<sub>2</sub> artefact of up to 0.63 pptV.  
285 However, these measurements were made using a thermostated inlet system with reactive  
286 HONO stripping, where loss of HONO to the sample lines is minimised. The NO<sub>x</sub> instrument  
287 at the CVAO samples at the end of the glass manifold making it highly likely that a significant  
288 fraction of HONO is lost on the manifold before the air is introduced to the NO<sub>x</sub> instrument  
289 due to the high surface reactivity of HONO (Pinto et al., 2014; Syomin and Finlayson-Pitts,  
290 2003). Thus, we regard the potential HONO-induced artefact of 0.63 pptV as an upper limit.  
291 No other potential photolytic artefacts have been measured at the CVAO, however using the

292 GEOS-Chem model (see section 3.2.2) we calculated seasonal cycles of 20 potential interfering  
293 compounds at the CVAO (Figure S7). None of these compounds exhibit major seasonal  
294 differences, indicating that any measurement artefact will be fairly constant across the year.  
295 The contribution from photolytic degradation of compounds other than HONO is predicted to  
296 be less than 0.05 pptV using the estimated conversion efficiency of each compound in Table 3  
297 and the modelled mixing ratios at the CVAO.

298 Peroxyacetyl nitrate (PAN) is produced in polluted areas and transported to remote  
299 regions, where it can thermally decompose into peroxy radicals and NO<sub>2</sub>. 5.8% of the available  
300 PAN has been shown to thermally decompose in blue light converters (BLC) switched on 40%  
301 of the time (Reed et al., 2016). This can cause significant overestimations of NO<sub>2</sub> in colder  
302 regions where PAN can build up in the atmosphere due to its long lifetime (Kleindienst, 1994),  
303 however, in warmer regions such as Cabo Verde the overestimation will be substantially lower  
304 due to the much shorter lifetime (~ 40-230 minutes at 25°C) (Bridier et al., 1991; Kleindienst,  
305 1994), and hence lower concentration of PAN. At the CVAO, PAN ~~was has been~~ measured in  
306 February 2020 using gas chromatography as described by Whalley et al. (Whalley et al., 2004),  
307 however, all measurements were below the limit of detection (LOD) of 6 pptV. We measured  
308 the temperature increase of the air within an identical photolytic converter (PLC) to the one  
309 used at the CVAO to be less than 1°C in the laboratory, suggesting a minimal shift in the PAN  
310 equilibrium in ambient air. We calculate an increase in NO<sub>2</sub> of 0.28 pptV arising from 6 pptV  
311 of PAN when increasing the temperature from 298 K to 299 K. The photolytic converter (PLC)  
312 used at the CVAO is only switched on 20% of the time, so a thermal decomposition efficiency  
313 of 5% for PAN is used to estimate a potential artefact of 0.3 pptV from PAN. Combining  
314 photolytic and thermal artefact contributions gives a maximum potential NO<sub>2</sub> artefact of 0.957  
315 pptV at the CVAO, which is within the uncertainty previously reported for the NO<sub>2</sub>  
316 measurements, ~~see Table 2~~ (Andersen et al., 2021), as shown in Table 2.

317

## 318 3.2 Modelling

### 319 3.2.1 Chemical Box Modelling

320 A tailored zero-dimensional chemical box model of the lower atmosphere,  
321 incorporating a subset of the Master Chemical Mechanism (MCM v3.3.1) (Jenkin et al., 2015)  
322 into the AtChem2 modelling toolkit (Sommariva et al., 2020), was used to estimate  
323 concentrations of OH, HO<sub>2</sub> and RO<sub>2</sub> and daily chemical production and loss of O<sub>3</sub> at the CVAO.

324 The MCM describes the detailed atmospheric chemical degradation of 143 VOCs, through  
325 17,500 reactions of 6900 species. More details can be found on the MCM website  
326 (<http://mcm.york.ac.uk>, last access: 4<sup>th</sup> March 2022). A fixed deposition rate of  $1.2 \times 10^{-5} \text{ s}^{-1}$   
327 was applied to all model generated species, giving them a lifetime of approximately 24 hours.  
328 The model was constrained to 34 observationally derived photolysis rates, temperature,  
329 pressure, and relative humidity, along with a range of observed chemical species, defined in  
330 Table 2.

331 While the box model is constrained to a variety of VOCs, which are expected to be the  
332 most dominant at the CVAO, it is only constrained to two oxygenated VOCs (OVOCs);  
333 methanol and acetone, due to the lack of reliable measurements of other OVOCs. Acetaldehyde  
334 and formaldehyde are expected to be the dominant OVOCs not constrained in the box model.  
335 Acetaldehyde from the ATom aircraft campaigns in October 2017, May 2018, and August 2018  
336 show levels of between ~150 and ~250 pptV (Wofsy et al., 2021), which agrees well with  
337 average observations of 180 pptV in the northern hemisphere over the Atlantic Ocean (Yang  
338 et al., 2014). Formaldehyde measured at the CVAO in 2006-2007 varied from 350 to 550 pptV  
339 (Mahajan et al., 2011). Compared to using the levels generated by the box model of ~8 pptV  
340 of acetaldehyde and 270 pptV of formaldehyde, constraining these gases to 150 pptV and 450  
341 pptV, respectively, increases the total RO<sub>x</sub> levels by 3% from 52.7 pptV to 54.4 pptV. Thus,  
342 we consider that the major VOCs and OVOCs are constrained sufficiently well in the box  
343 model for the purpose of simulating HO<sub>2</sub> and RO<sub>2</sub> levels.

344

### 345 3.2.2 GEOS-Chem

346 Concentrations of 20 different chemical species were extracted every hour during 2019  
347 at nearest point in space and time from the GEOS-Chem model (v12.9.0,  
348 DOI:10.5281/zenodo.3950327). The v12.9.0 model as described by Wang et al. (2021) was run  
349 at a nested horizontal resolution of 0.25x0.3125 degrees over the region (-32.0 to 15.0 °E, 0.0  
350 to 34.0 °N), with boundary conditions provided by a separate global model run spun up for one  
351 year and with acid uptake on dust considered as described by Fairlie et al. (2010) (Fairlie et al.,  
352 2010; Wang et al., 2021).

353

## 354 4 Results and Discussion

355 Monthly diurnal cycles of HO<sub>2</sub>, RO<sub>2</sub>, and OH were modelled by constraining the box  
356 model to the measurements described in Table 2 (except NO<sub>2</sub>) using hourly median  
357 concentrations for each month from July 2017 – June 2020 where all the trace gas  
358 measurements were available. When measured  $j\text{O}(^1\text{D})$  was not available, the hourly average  
359 from the same month across the other years was used. Calculated photolysis rates based on  
360 total solar radiation (see supplementary) were used up to December 2019 for all other  
361 photolysis rates than  $j\text{O}(^1\text{D})$ .

362 The modelled OH, HO<sub>2</sub> and RO<sub>2</sub> concentrations agree reasonably well with previous  
363 measurements from short term field campaigns based at the CVAO and from various cruises  
364 in the Atlantic Ocean (see Figure 2). All the previous measurements of RO<sub>x</sub> (HO<sub>2</sub> + RO<sub>2</sub>)  
365 shown in Figure 2 were conducted using the chemical amplifier technique, which is subject to  
366 high uncertainties due to the challenges described above. The box modelled RO<sub>2</sub> shows a strong  
367 correlation with the measured  $j\text{O}(^1\text{D})$ , but no correlation to CO (pollution tracer) or CH<sub>4</sub>, which  
368 is expected to be the primary precursor. Daily diurnal cycles of RO<sub>2</sub> and HO<sub>2</sub> for 9 days in  
369 August 2017, 12 days in October 2017, and 20 days in January 2018 were modelled to  
370 investigate their daily variability (see Figure S8). Seasonal differences can be observed from  
371 the daily outputs, but no major day to day changes within a given month.

372

### 373 4.1 Comparison of measured and PSS NO<sub>2</sub> concentrations

374 Daily midday (12.00-15.00 UTC, local+1) NO<sub>2</sub> mixing ratios were calculated from the  
375 Leighton ratio using equation II ( $[\text{NO}_2]_{\text{PSS}}$ ), the measured NO, O<sub>3</sub>, and  $j\text{NO}_2$  and  $k_1 = 2.07 \times$   
376  $10^{-12} \times e^{(-1400/T)}$  (Atkinson et al., 2004) for a three-year period (July 2017 – June 2020).  
377 Individual uncertainties of  $[\text{NO}_2]_{\text{PSS}}$  were determined to be  $4.20 \pm 3.74$  pptV ( $1\sigma$ ) for each day  
378 using the  $2\sigma$  hourly uncertainties for all the used measurements, which is very similar to the  
379 uncertainty of hourly measured  $[\text{NO}_2]$  (Table 2). Figure 3A shows that  $[\text{NO}_2]_{\text{PSS}}$  significantly  
380 underestimates the measured NO<sub>2</sub>, indicating that additional oxidants are needed to convert  
381 NO into NO<sub>2</sub>. Daily midday values of  $[\text{NO}_2]_{\text{PSS ext.}}$  were calculated using equation III, where a  
382 midday average of each modelled monthly diurnal cycle of HO<sub>2</sub> and RO<sub>2</sub> in Figure 2 was used  
383 for all days of their respective month together with previous yearly averaged midday  
384 measurements of IO ( $1.4 \pm 0.8$  pptV,  $1\sigma$ ) and BrO ( $2.5 \pm 1.1$  pptV,  $1\sigma$ ) (Mahajan et al., 2010;

385 Read et al., 2008) at the CVAO. RO<sub>2</sub> was assumed to be equivalent to CH<sub>3</sub>O<sub>2</sub>, making  $k_4 = 2.3$   
386  $\times 10^{-12} \times e^{(360/T)}$ ,  $k_5 = 3.45 \times 10^{-12} \times e^{(270/T)}$ ,  $k_6 = 7.15 \times 10^{-12} \times e^{(300/T)}$ , and  $k_7 = 8.7 \times 10^{-12} \times$   
387  $e^{(260/T)}$  (Atkinson et al., 2004). Uncertainties for each estimation of [NO<sub>2</sub>]<sub>PSS ext.</sub> were  
388 determined using the calculated 2σ hourly uncertainties on the measurements and a 20%  
389 uncertainty on all rate coefficients. This gives a total average uncertainty of  $4.90 \pm 4.12$  pptV  
390 (1σ), excluding any uncertainties in [HO<sub>2</sub>] and [RO<sub>2</sub>]. [NO<sub>2</sub>]<sub>PSS ext.</sub> was calculated using a  
391 midday average of the modelled monthly [HO<sub>2</sub>] and [RO<sub>2</sub>] in Figure 2 as well as the modelled  
392 daily midday averages from the diurnal cycles in Figure S8 for August 2017, October 2017,  
393 and January 2018. A scatter plot of monthly vs daily calculated [NO<sub>2</sub>]<sub>PSS ext.</sub> around the 1:1 line  
394 (see Figure S9) verifies the use of monthly calculated [HO<sub>2</sub>] and [RO<sub>2</sub>] for the remaining  
395 analyses.

396 Figure 3B shows that the agreement between measured and predicted NO<sub>2</sub> and [NO<sub>2</sub>]<sub>PSS</sub>  
397 ext. was improved significantly by including modelled additional oxidants— with the slope of  
398 the linear fit increasing from 0.48 to 0.71. The coefficient of determination was similar for both  
399 plots: Figure 3A,  $r^2 = 0.81$  and Figure 3B,  $r^2 = 0.77$ . At NO<sub>2</sub>-mixing ratios below 20 pptV, the  
400 scatter of [NO<sub>2</sub>]<sub>PSS ext.</sub> vs [NO<sub>2</sub>]<sub>Obs.</sub> was close to the 1:1 line, however, at higher NO<sub>2</sub>-mixing  
401 ratios [NO<sub>2</sub>]<sub>PSS ext.</sub> under-predicts the observed NO<sub>2</sub>-mixing ratio by on average 9.5 pptV. NO<sub>2</sub>  
402 mixing ratios above 20 pptV are predominantly observed at the CVAO from December-  
403 February (Andersen et al., 2021), which coincides with the arrival of predominantly African  
404 air to the site (see Figure 1).

405 We next investigate whether the effects of seasons and the mixing ratio abundance of  
406 NO influences the ability of the full PSS equation (equation III) to predict NO<sub>2</sub>. Daily  
407 midday averages of [NO<sub>2</sub>]<sub>Obs. / [NO<sub>2</sub>]<sub>PSS ext.</sub> are plotted as a function of NO in Figure 4. A ratio  
408 of 1 would be expected if all relevant reaction mechanisms have been taken into account. The  
409 deviations from 1 in the ratio can be observed to increase with decreasing NO mixing ratio  
410 during March-December. The dashed lines in Figure 4 visualise the effect of a constant NO<sub>2</sub>  
411 artefact of 0.957 pptV (our calculated upper limit) on the [NO<sub>2</sub>]<sub>Obs. / [NO<sub>2</sub>]<sub>PSS ext.</sub> ratio, showing  
412 that the artefact, while small, can explain some of this observed trend. However, only a small  
413 dependence on the NO mixing ratio is seen for January and February, where enhancements of  
414 [NO<sub>2</sub>]<sub>Obs. / [NO<sub>2</sub>]<sub>PSS ext.</sub> above 1 continue out to 10 pptV of NO. At Hohenpeissenberg, Germany,  
415 similar trends with increasing NO<sub>2</sub>/NO ratio with decreasing NO have been observed, which  
416 were partly explained by measurement uncertainty in NO and partly by the PSS not being  
417 established after being perturbed by NO<sub>x</sub> emissions or variable jNO<sub>2</sub> (Mannschreck et al.,</sub></sub></sub>



418 2004). An opposite trend to that observed here and at Hohenpeissenberg was observed over the  
419 South Atlantic Ocean, with increasing deviations in  $[\text{NO}_2]_{\text{Obs.}}/[\text{NO}_2]_{\text{PSS ext.}}$  with increasing  $\text{NO}_2$   
420 from 3-20 pptV (Hosaynali Beygi et al., 2011), which was explained by a missing photolytic  
421 oxidation process.

422

## 423 4.2 $\text{NO}_2$ Artefact or Missing Oxidant?

424 Deviations between  $[\text{NO}_2]_{\text{Obs.}}$  and  $[\text{NO}_2]_{\text{PSS ext.}}$  are usually attributed to an unaccounted  
425 artefact in the  $\text{NO}_2$  measurements or a missing oxidant converting  $\text{NO}$  into  $\text{NO}_2$  (Bradshaw et  
426 al., 1999; Carpenter et al., 1998; Crawford et al., 1996; Hauglustaine et al., 1999; Hauglustaine  
427 et al., 1996; Hosaynali Beygi et al., 2011; Volz-Thomas et al., 2003). As discussed above, we  
428 show that below 5 pptV of ambient  $\text{NO}$ , our calculated maximum  $\text{NO}_2$  artefact of 0.957 pptV  
429 starts to have an impact on the  $[\text{NO}_2]_{\text{Obs.}}/[\text{NO}_2]_{\text{PSS ext.}}$  ratio, however, it is not enough to explain  
430 the enhancements observed, especially in wintertime at the CVAO.

431 The production of  $\text{RO}_2$  and  $\text{HO}_2$  radicals is dependent on the abundance of their VOC  
432 and CO precursors as well as on photochemical activity. To investigate whether the availability  
433 of VOCs, CO or sunlight was related to the discrepancy between  $[\text{NO}_2]_{\text{Obs.}}$  and  $[\text{NO}_2]_{\text{PSS ext.}}$ ,  
434 ~~Figure 4 was replotted by colouring boxplots of the  $[\text{NO}_2]_{\text{Obs.}}/[\text{NO}_2]_{\text{PSS ext.}}$  ratio are plotted as a~~  
435 ~~function of intervals of the mixing ratio of a different particular precursors and  $j\text{NO}_2$  (Figure~~  
436 ~~5). The high deviations in  $[\text{NO}_2]_{\text{Obs.}}/[\text{NO}_2]_{\text{PSS ext.}}$  at  $\text{NO} > 2.5$  pptV can be observed to be~~  
437 ~~associated with higher measured mixing ratios of CO, ethane, and acetylene, and lower midday~~  
438  ~~$j\text{NO}_2$ , however, it should be noted that the variation in midday photolysis rates at the CVAO~~  
439 ~~over the year is relatively small. No obvious trend can be observed in the dependence on  $j\text{NO}_2$ ,~~  
440 ~~contrast to Hosaynali Beygi et al. (2011), who observed increasing deviations in~~  
441  ~~$[\text{NO}_2]_{\text{Obs.}}/[\text{NO}_2]_{\text{PSS ext.}}$  with increasing  $j\text{NO}_2$ . However, it should be noted that midday  $j\text{NO}_2$  at~~  
442 ~~the sub-tropical CVAO shows relatively little seasonal variation. At similar  $j\text{NO}_2$  as observed~~  
443 ~~at the CVAO at midday ( $>0.007 \text{ s}^{-1}$ ), Hosaynali Beygi et al. observed the largest deviations in~~  
444  ~~$[\text{NO}_2]_{\text{Obs.}}/[\text{NO}_2]_{\text{PSS ext.}}$  (Hosaynali Beygi et al., 2011). For the high enhancements in~~  
445  ~~$[\text{NO}_2]_{\text{Obs.}}/[\text{NO}_2]_{\text{PSS ext.}}$  at  $\text{NO} < 2.5$  pptV at the CVAO, the trends are not as clear. The mixing~~  
446 ~~ratios of CO can be observed to remain enhanced, however, high  $j\text{NO}_2$  is seen at  $\text{NO} < 2.5$~~   
447 ~~pptV while the ethane and acetylene mixing ratios are lower than when  $\text{NO} > 2.5$  pptV. It is~~  
448 ~~important to note though that the deviation at very low  $\text{NO}$  can on most days be explained by~~  
449 ~~the measurement uncertainty in  $\text{NO}$  ( $\sim 1.4$  pptV). Figure 5 shows that the abundances of ethene~~



450 and propene, both of which have atmospheric lifetimes of less than 3 days, do not seem to  
451 affect the deviation of  $[\text{NO}_2]_{\text{Obs.}}/[\text{NO}_2]_{\text{PSS ext.}}$  from 1. Conversely, high abundances of CO,  
452 ethane, and acetylene, which all have atmospheric lifetimes above 6 weeks (Atkinson et al.,  
453 2006), are observed to be associated with higher  $[\text{NO}_2]_{\text{Obs.}}/[\text{NO}_2]_{\text{PSS ext.}}$  ratios. This could  
454 indicate that long-range transport of pollutants supplies additional peroxy radicals (or other NO  
455 to  $\text{NO}_2$  oxidants) at the CVAO, which are not predicted from known sources and  
456 photochemistry.

457 To further evaluate the impact of pollution,  $[\text{NO}_2]_{\text{Obs.}}/[\text{NO}_2]_{\text{PSS ext.}}$  was separated into  
458 three categories based on CO mixing ratios;  $\text{CO} < 90$  ppbV,  $90 \text{ ppbV} < \text{CO} < 100$  ppbV, and  
459  $\text{CO} > 100$  ppbV. The deviations of  $[\text{NO}_2]_{\text{Obs.}}/[\text{NO}_2]_{\text{PSS ext.}}$  from 1 increase with increasing [CO],  
460 with 50<sup>th</sup> (25<sup>th</sup>-75<sup>th</sup>) percentiles of 1.10 (0.82 -1.37) for  $\text{CO} < 90$  ppbV, 1.20 (0.97-1.54) for  
461  $90 \text{ ppbV} < \text{CO} < 100$  ppbV, and 1.50 (1.18-1.78) for  $\text{CO} > 100$  ppbV. The small deviation from  
462 1, which is within the uncertainty of our measurements (see below), for  $\text{CO} < 90$  ppbV is strong  
463 evidence that fundamental oxidation process in ultra-clean marine air, where the main  
464 precursors of  $\text{RO}_2$  and  $\text{HO}_2$  are  $\text{CH}_4$  and CO giving  $\text{CH}_3\text{O}_2$  and  $\text{HO}_2$ , respectively, are well  
465 understood.

466 An  $\text{NO}_2$  artefact of 0.7 pptV would reduce the ratio of 1.10 to 1.00 in air masses with  
467  $\text{CO} < 90$  ppbV. Since the minimum value of the artefact is 0 pptV (if there was no conversion  
468 of interferent compounds to NO or  $\text{NO}_2$ ), and our estimated upper limit is 0.97 pptV, we  
469 therefore consider it a reasonable assumption that the average  $\text{NO}_2$  artefact of our instrument  
470 at the CVAO is 0.7 pptV. We make the simple *a priori* assumption that this applies across all  
471 measurements during the period of analyses. Such an artefact is insignificant when considering  
472 total  $\text{NO}_x$  concentrations, however, it has a non-negligible impact when investigating  $\text{NO}_2/\text{NO}$   
473 ratios in this very low  $\text{NO}_x$  environment.

474 Subtracting 0.7 pptV from all the  $\text{NO}_2$  observations results in median (25<sup>th</sup>-75<sup>th</sup>  
475 percentiles) ratios of 1.00 (0.76-1.29) for  $\text{CO} < 90$  ppbV, 1.14 (0.89-1.47) for  $90 \text{ ppbV} < \text{CO}$   
476  $< 100$  ppbV, and 1.42 (1.12-1.68) for  $\text{CO} > 100$  ppbV (Table 4). A student's t-test was  
477 performed to evaluate whether the two categories where  $\text{CO} < 90$  ppbV and  $\text{CO} > 100$  ppbV  
478 were significantly different. A mean and standard deviation of 1.06 and 0.42 for  $\text{CO} < 90$  ppbV  
479 and 1.45 and 0.61 for  $\text{CO} > 100$  ppbV results in a t-value of 6.59, which makes the two  
480 categories statistically different. Distributions of each category are plotted in Figure 6A. When  
481 CO is between 90 and 100 ppbV, the distribution of  $[\text{NO}_2]_{\text{Obs.}}/[\text{NO}_2]_{\text{PSS ext.}}$  shows the highest

482 occurrences at ratios of ~1 and ~1.5. When CO > 100 ppbV, it is evident that either additional  
483 oxidants are needed to convert NO to NO<sub>2</sub>, or an additional NO<sub>2</sub> artefact of the order of 4.4  
484 pptV is present in these air masses. As an artefact of 0.7 pptV has already been subtracted, and  
485 measurements of HONO and PAN and modelled mixing ratios of halogen nitrates indicate a  
486 fairly stable artefact across the year, 4.4 pptV of additional artefact seems highly unlikely. This  
487 leaves the possibility of a missing oxidant when the sampled air is enhanced in CO.

488 Using equation (IV) and (V), the required RO<sub>x</sub> (RO<sub>2</sub> + HO<sub>2</sub>) and XO (IO + BrO)  
489 concentrations needed to reconcile [NO<sub>2</sub>]<sub>Obs.</sub> with [NO<sub>2</sub>]<sub>PSS ext</sub> can be estimated using  $k_{4,5} = 2.3$   
490  $\times 10^{-12} \times e^{(360/T)}$  and  $k_{6,7} = 8.7 \times 10^{-12} \times e^{(260/T)}$  (Atkinson et al., 2004). Our calculations are based  
491 on two scenarios: (1) that the measured [BrO] and [IO] are correct and there is unaccounted  
492 for missing RO<sub>x</sub>, or (2) that the modelled [RO<sub>x</sub>] is correct and there is more missing [XO] than  
493 measured. Due to the similar rate coefficients for IO and BrO reacting with NO, a combined  
494 XO can be estimated. The results are summarised in Table 4 based on the three CO categories.  
495 The median required RO<sub>x</sub> was determined to be 65.0 (33.68 - 112.5, 25<sup>th</sup>-75<sup>th</sup> percentile) pptV  
496 and 109.7 (63.14 - 149.5, 25<sup>th</sup>-75<sup>th</sup> percentile) pptV for 90 ppbV < CO < 100 ppbV and CO >  
497 100 ppbV, respectively. RO<sub>x</sub> measurements during the ALBATROSS cruise varied from 40-  
498 80 pptV while in the North Atlantic, however, with a reported uncertainty of 25% (1σ) they  
499 could be as high as 100 pptV (Burkert et al., 2001). Such concentrations are comparable to the  
500 required median RO<sub>x</sub> in this study of 109.7 pptV when CO > 100 ppbV. The uncertainty  
501 reported for ALBATROSS is similar to many other studies which have reported 10-36%  
502 uncertainty on chemical amplification RO<sub>x</sub> measurements (Cantrell et al., 1997; Clemitshaw et  
503 al., 1997; Handisides et al., 2003; Hernández et al., 2001; Hosaynali Beygi et al., 2011; Volz-  
504 Thomas et al., 2003), however, a recent study in the Pearl River Delta reported an uncertainty  
505 of 60% (1σ) (Ma et al., 2017). This combined with measurements up to ~150 pptV of RO<sub>x</sub> in  
506 the South Atlantic Ocean (Hosaynali Beygi et al., 2011) indicates that our required RO<sub>x</sub> levels  
507 of ~ 100 pptV may not be unrealistic in the MBL.

508 The median required RO<sub>x</sub> ([RO<sub>x</sub>]<sub>PSS</sub>) can be observed to be ~2.5 times higher than ~~these~~  
509 levels estimated using the box modelled for air masses where CO > 100 ppbV, whereas the  
510 required [XO] is a factor of ~6.5 higher than previous observations at the CVAO (Mahajan et  
511 al., 2010; Read et al., 2008) ~~due to the lower rate coefficients for halogen oxides with NO.~~  
512 Across the three categories, the daily median ratio of [RO<sub>x</sub>]<sub>PSS</sub>/[RO<sub>x</sub>]<sub>Model</sub> is 1.5, which is  
513 similar to those observed in previous studies both in remote and rural regions (see Table 1).  
514 The additional missing XO required to reconcile [NO<sub>2</sub>]<sub>Obs.</sub> with [NO<sub>2</sub>]<sub>PSS ext.</sub> was determined for

515 each CO category by subtracting the previous measured average concentration of 3.9 pptV (2.5  
 516 pptV BrO + 1.4 pptV IO) (Read et al., 2008) from the required XO. Since CO, the main  
 517 precursor for HO<sub>2</sub>, is constrained by measurements in the model, the calculated [HO<sub>2</sub>] is  
 518 assumed to be correct. Thus, we estimate the required and unaccounted for RO<sub>2</sub>  
 519 assuming it is all in the form of CH<sub>3</sub>O<sub>2</sub> from:

$$520 \quad [\text{RO}_2]_{\text{Required}} = \frac{j\text{NO}_2[\text{NO}_2] - (k_1[\text{O}_3] + k_5[\text{HO}_2] + k_6[\text{IO}] + k_7[\text{BrO}])[\text{NO}]}{k_4[\text{NO}]} \quad (\text{VIII})$$

$$521 \quad [\text{RO}_2]_{\text{UnaccountedMissing}} = \frac{j\text{NO}_2[\text{NO}_2] - (k_1[\text{O}_3] + k_5[\text{HO}_2] + k_6[\text{IO}] + k_7[\text{BrO}])[\text{NO}]}{k_4[\text{NO}]} - [\text{RO}_2]_{\text{model}}$$

522 (IX)

523 Figures 6B and C, show that the unaccounted for RO<sub>2</sub> or XO level increases  
 524 with increasing [CO], reaching a median of 61.3 pptV and 22.7 pptV, respectively, for air  
 525 masses where CO > 100 ppbV, which is approximately 2.2 times the box modelled RO<sub>2</sub> and  
 526 5.5 times the measured XO in the same air masses. Such an increase in peroxy radicals would,  
 527 under more polluted conditions, cause a major increase in O<sub>3</sub> production during a day (Volz-  
 528 Thomas et al., 2003). We next examine the impact of additional RO<sub>2</sub> on the net O<sub>3</sub>  
 529 production rate in Cabo Verde.

### 531 4.3 Chemical O<sub>3</sub> Loss

532 The daily chemical loss of O<sub>3</sub> between 09.30 (09.00-10.00) and 17.30 (17.00-18.00)  
 533 UTC was used to evaluate whether the PSS-derived [RO<sub>2</sub>] was consistent with the net chemical  
 534 destruction of O<sub>3</sub> at the CVAO. As discussed above, the measured O<sub>3</sub> mixing ratio in the MBL  
 535 is affected by loss mechanisms in the form of photolysis, reactions with HO<sub>x</sub> and halogens, and  
 536 deposition, and by production through NO<sub>2</sub> photolysis and by entrainment from the O<sub>3</sub>-  
 537 enriched free troposphere. Due to the very stable meteorological condition of the MBL, the  
 538 variability in entrainment and deposition between night and day is expected to be negligible  
 539 (Ayers and Galbally, 1995; Ayers et al., 1992; Read et al., 2008). A combined  
 540 entrainment/deposition term can therefore be estimated from night time O<sub>3</sub> measurements,  
 541 when there is no photochemical production or loss. An hourly entrainment/deposition term was  
 542 determined for each month using the average change in O<sub>3</sub> between 22.30 (22.00-23.00) and  
 543 03.30 (03.00-04.00), and found to vary from 0.18 ppbV h<sup>-1</sup> in January to 0.35 ppbV h<sup>-1</sup> in May,  
 544 which is in good agreement with previous measurements at the CVAO of 0.18-0.48 ppbV h<sup>-1</sup>

545 (Read et al., 2008). The observed daily change in O<sub>3</sub> ( $\Delta O_3$  obs.) (09.30-17.30) was determined  
546 to be  $-0.40 \pm 0.32$  ppbV h<sup>-1</sup> (1 $\sigma$ ) across the three years (2017-2020), which is almost identical  
547 to the  $-0.41 \pm 0.33$  ppbV h<sup>-1</sup> (1 $\sigma$ ) observed at the CVAO in 2007 (Read et al., 2008), but roughly  
548 2 times the daily  $\Delta O_3$  obs. in baseline air at Cape Grim ( $-0.24 \pm 0.32$  ppbV h<sup>-1</sup>, 1 $\sigma$ ) and Mace  
549 Head ( $-0.20 \pm 0.21$  ppbV h<sup>-1</sup>, 1 $\sigma$ ) (Carpenter et al., 1997) and 2-40 times the modelled O<sub>3</sub> loss  
550 at Mauna Loa ( $-0.01$  to  $-0.21$  ppbV h<sup>-1</sup>) (Cantrell et al., 1996; Ridley et al., 1992).

551 By subtracting the monthly average entrainment/deposition term from the observed  
552 daily  $\Delta O_3$ , the daily chemical loss of O<sub>3</sub>,  $\Delta O_3$  chem., is obtained. The observations were filtered  
553 to exclude periods where the change in CO concentration over the interval period,  $\Delta CO$ , was  
554 outside 1 standard deviation of the mean  $\Delta CO$ , to avoid the  $\Delta O_3$  determination being affected  
555 by changing air masses. The resulting observed chemical loss of O<sub>3</sub> is averaged by month and  
556 plotted in black in Figure 7.  $\Delta O_3$  chem. can be observed to follow photochemical activity, with  
557 the lowest  $\Delta O_3$  chem. in October-February, where the lowest photolysis rates are measured (see  
558 supplementary and Table 2) and highest  $\Delta O_3$  chem. in March-May and September. A small  
559 decrease in  $\Delta O_3$  chem. in June-August occurred simultaneously to the small drop in photolysis  
560 rates in June-August. Overall,  $\Delta O_3$  chem. varied from  $-0.48$  ppbV h<sup>-1</sup> in January to  $-0.88$  ppbV h<sup>-1</sup>  
561 in May.

562 In order to evaluate whether these observationally-derived chemical loss rates of O<sub>3</sub> are  
563 consistent with PSS-derived peroxy radical concentrations,  $\Delta O_3$  chem. was estimated using a  
564 chemical box model incorporating the MCM, as described in section 3.2.1. The model was  
565 constrained to all the measurements described in Table 2, except NO<sub>2</sub> and O<sub>3</sub>, which were left  
566 unconstrained.  $\Delta O_3$  chem. was simulated with [box](#) modelled [RO<sub>2</sub>] and [HO<sub>2</sub>], with (blue line in  
567 Figure 7) and without (grey in Figure 7) inclusion of the halogen chemistry described in Table  
568 S1, allowing an evaluation of the O<sub>3</sub> loss due to halogens, as previously discussed by Read et  
569 al. (2008). Simulations were also performed with [CH<sub>3</sub>O<sub>2</sub>] constrained to the required RO<sub>2</sub>,  
570 [box](#) modelled [HO<sub>2</sub>] and including halogen chemistry (orange in Figure 7). In model runs with  
571 halogen chemistry, BrO and IO were constrained to previously measured annual averages  $\pm$   
572 reported uncertainties (blue shaded area in Figure 7) (Read et al., 2008). Diurnal cycles of the  
573 required RO<sub>2</sub> were constructed using the median of the daily midday averages for each month  
574 determined using equation (VIII) for the peak concentration at midday, 1 pptV overnight and  
575 interpolating linearly in between.

576 Figure 7 shows that all three modelled  $\Delta O_3$  chem. exhibited very similar seasonality as  
577 the observed  $\Delta O_3$  chem.. The difference between running the box model with and without  
578 halogen chemistry was  $0.24 \pm 0.02$  ppbV h<sup>-1</sup> (1 $\sigma$ ), which is almost equivalent to the results of  
579 Read et al. (2008) from the CVAO of  $0.23 \pm 0.05$  ppbV h<sup>-1</sup> (1 $\sigma$ ). From May-December, the box  
580 modelled  $\Delta O_3$  chem. was almost identical whether using modelled RO<sub>2</sub> or constraining CH<sub>3</sub>O<sub>2</sub>  
581 to the required RO<sub>2</sub>, and both were very similar to observed  $\Delta O_3$  chem.. The largest difference in  
582  $\Delta O_3$  chem. between using box modelled RO<sub>2</sub> and constraining CH<sub>3</sub>O<sub>2</sub> is observed in January  
583 where the difference reached  $0.09$  ppbV h<sup>-1</sup>, however, this is caused by constraining CH<sub>3</sub>O<sub>2</sub> to  
584 100 pptV, which is 5 times more than the modelled RO<sub>2</sub>. The average difference between the  
585 observed and box modelled  $\Delta O_3$  chem. is  $0.06 \pm 0.07$  ppbV h<sup>-1</sup> (1 $\sigma$ ) when constraining CH<sub>3</sub>O<sub>2</sub> to  
586 the required RO<sub>2</sub> and  $0.04 \pm 0.07$  ppbV h<sup>-1</sup> (1 $\sigma$ ) when using box modelled RO<sub>2</sub>.

587 Overall, the very small differences in modelled  $\Delta O_3$  chem. whether including the  
588 unaccounted for “missing RO<sub>2</sub>” or not are a function of the highly NO<sub>x</sub>-limited conditions of  
589 the remote MBL, where O<sub>3</sub> production is relatively insensitive to the mixture and abundance  
590 of peroxy radicals (Sillman, 1999). Thus, although our analysis shows that peroxy radicals  
591 with the equivalent O<sub>3</sub> production potential as CH<sub>3</sub>O<sub>2</sub> cannot be ruled out as the missing oxidant  
592 in marine air masses with aged pollution, neither does it provide robust evidence that the  
593 missing oxidant is O<sub>3</sub>-producing. Nevertheless, the deviation between PSS-derived peroxy  
594 radicals in this study and previous measurements can potentially be explained by the difficulty  
595 in measuring peroxy radicals, as discussed above. This would have important consequences for  
596 our understanding of O<sub>3</sub> production under higher NO<sub>x</sub> conditions.

597

## 598 5 Conclusions

599 In the remote MBL (CO < 90 ppbV, NO<sub>x</sub> < 43 pptV (90<sup>th</sup> percentile = 23 pptV)) we  
600 have shown that the observed NO<sub>2</sub>/NO ratio is consistent with fundamental photochemical  
601 theory, and that neither missing oxidants nor deviations of the photostationary state are required  
602 to reconcile observations with the calculated NO<sub>2</sub>/NO ratio. This is to our knowledge the first  
603 time this has been shown in a low NO<sub>x</sub> environment. However, observed NO<sub>2</sub> levels became  
604 increasingly higher than predicted as the CO mixing ratio increased and the air more influenced  
605 by long range transport of air pollution in winter. A detailed analysis of potential NO<sub>2</sub>  
606 measurement artefacts at the CVAO showed that such artefacts were unlikely to account for  
607 these deviations, thus we evaluated the case for a missing NO to NO<sub>2</sub> oxidant. The required

608 oxidant in air masses with  $\text{CO} > 100$  ppbV reached a median of 109.7 pptV when treated as  
609  $\text{CH}_3\text{O}_2$ . These levels are  $\sim 2.5$  times higher than both our [box](#) modelled  $\text{RO}_x$  ( $\text{RO}_2 + \text{HO}_2$ ) and  
610 previous measurements of  $\text{RO}_x$  measured by chemical amplification at the CVAO. However,  
611 chemical amplification measurements are known to be highly uncertain due to the difficulty in  
612 determining the chain length of the mixture of  $\text{RO}_2$  in the ambient matrix, and we note that the  
613 [box](#) modelled  $\text{O}_3$  production at the CVAO, with the inclusion of these additional peroxy  
614 radicals, did not deviate significantly from the observed  $\text{O}_3$  production. Overall, we conclude  
615 that there is strong evidence for a missing oxidant in remote marine air impacted by long range  
616 transport of pollution, and that peroxy radicals cannot be ruled out as to their identity.

617

## 618 6 Acknowledgements

619 The authors would like to thank the UK Natural Environment Research Council/  
620 National Centre for Atmospheric Science (NERC/NCAS) through the Atmospheric  
621 Measurement and Observation Facility (AMOF) for funding the CVAO programme. STA's  
622 PhD was supported by the SPHERES Natural Environment Research Council (NERC)  
623 Doctoral Training Partnership (DTP), under grant NE/L002574/1. LJC acknowledges funding  
624 from the European Research Council (ERC) under the European Union's Horizon 2020 pro-  
625 gramme (project O3-SML; grant agreement no. 833290).

626

## 627 7 Author Contributions

628 Data analysis has been performed by STA. The box model has been run by BSN. Back  
629 trajectories have been modelled by MR. GEOS-Chem has been run by TS. The instruments at  
630 the CVAO have been run by STA, KAR, SP, JH, and LN. KAR and LKW have processed the  
631 spectral radiometer data. The manuscript has been written by STA, LJC, JDL, BSN, and KAR.

632

## 633 8 Additional Information

634 The authors declare that they have no competing interests.

635

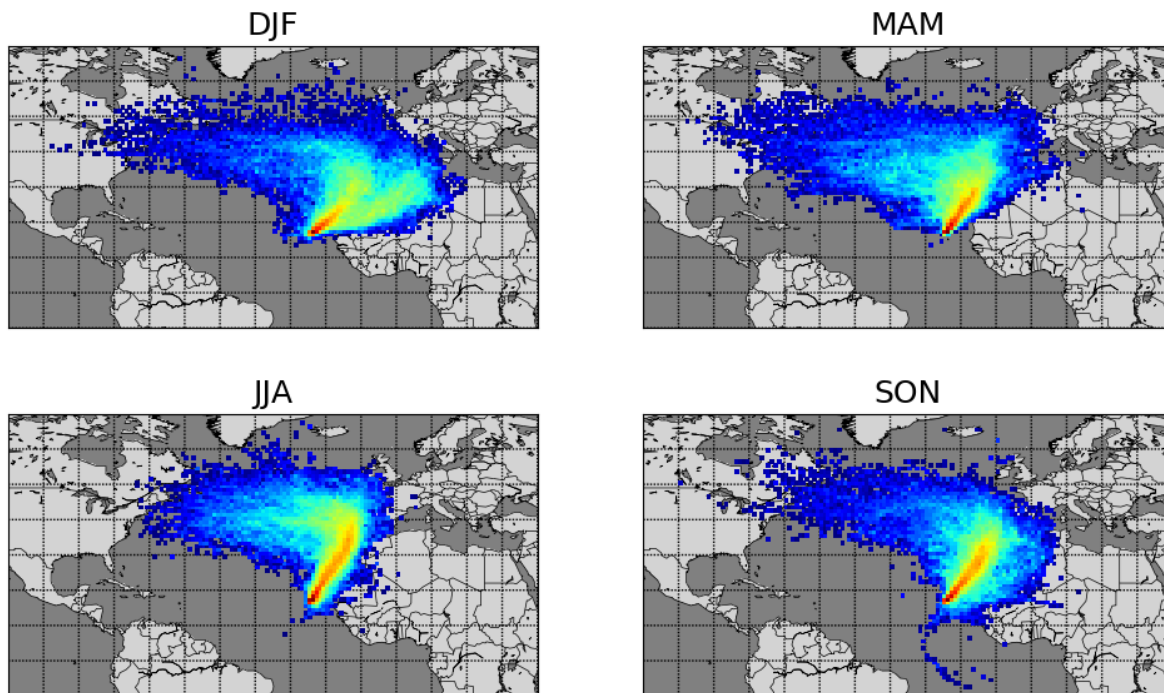
636 **8.1 Data availability:**

637 NO<sub>x</sub>, VOCs, meteorological data, CO and O<sub>3</sub>: WDCRG (World Data Centre for  
638 Reactive Gases)/Norwegian Institute for Air Research (NILU) EBAS database ([EBAS](http://ebas.nilu.no)  
639 [nilu.no](http://ebas.nilu.no))

640 CH<sub>4</sub> and CO: [WDCGG \(World Data Centre for Greenhouse Gases\) \(kishou.go.jp\)](http://wddc.kishou.go.jp)

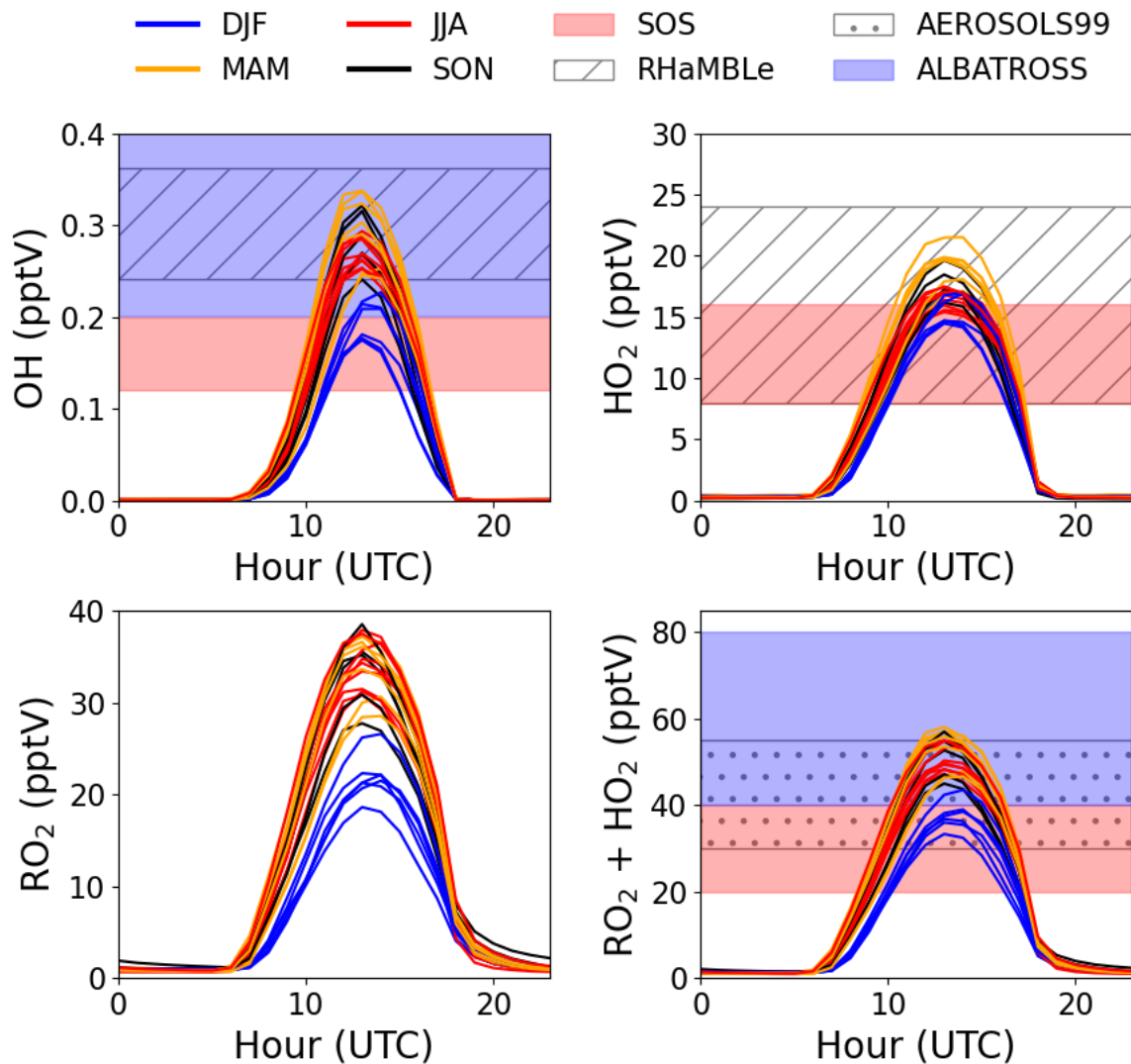


641 9 Figures



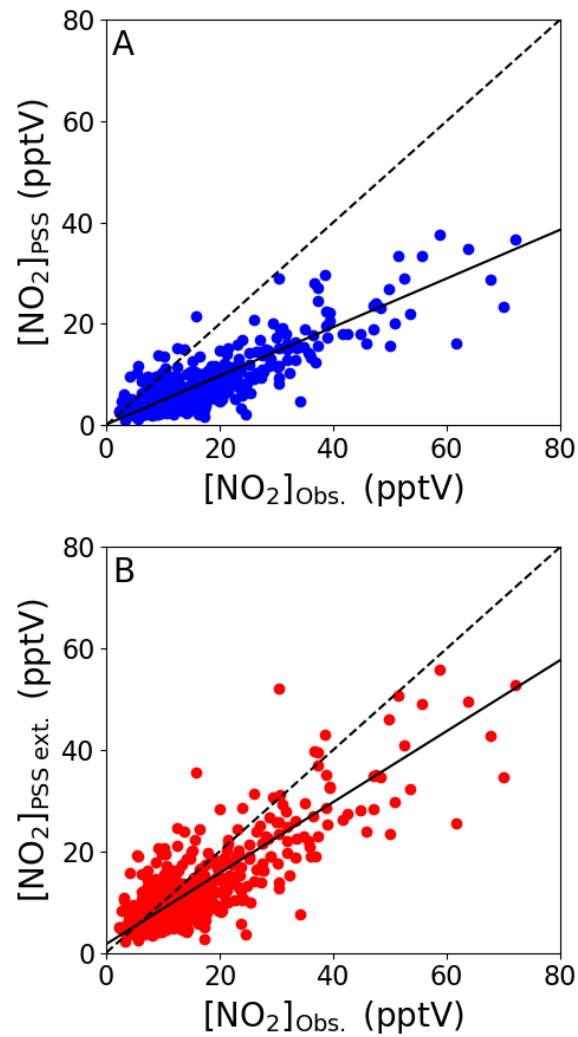
642

643 Figure 1: Seasonal average 10-day back trajectories for the CVAO. Locations of released  
644 particles are plotted on a 1°x1° grid, determined using FLEXPART as described in Andersen  
645 et al. (2021).~~Seasonal average 10-day back trajectories for the CVAO determined using~~  
646 ~~FLEXPART as described in Andersen et al. (2021).~~

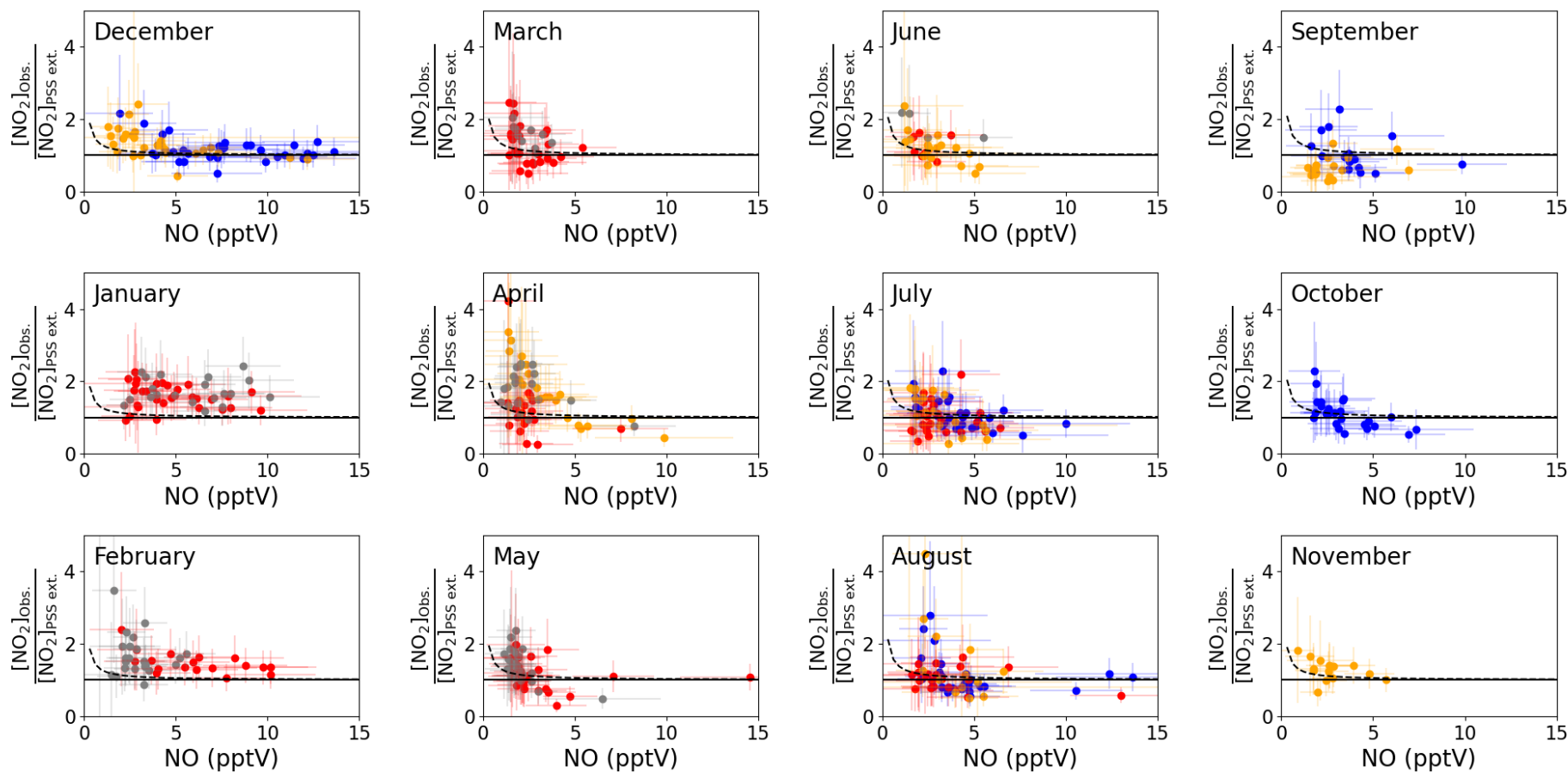


647

648 Figure 2: Average monthly diurnal cycles of modelled OH, HO<sub>2</sub>, RO<sub>2</sub>, and HO<sub>2</sub>+RO<sub>2</sub> coloured  
 649 by season compared to midday measurements during SOS (February, May, September, and  
 650 November) (Carpenter et al., 2010; Vaughan et al., 2012), RHaMBLe (May and June) (Whalley  
 651 et al., 2010), AEROSOLS99 (January and February) (Hernández et al., 2001), and  
 652 ALBATROSS (November and December) (Burkert et al., 2001).



655 Figure 3: Midday (12.00-15.00 UTC, local+1) daily averages of [NO<sub>2</sub>]<sub>PSS</sub> (A) and [NO<sub>2</sub>]<sub>PSS ext.</sub> (B) plotted against the observed NO<sub>2</sub> using measurements from July 2017 – June 2020. The black dashed lines show the 1:1 ratio and the solid black lines show the linear fit to the datapoints (A:  $0.48 \times [\text{NO}_2]_{\text{Obs.}} + 0.16$ , B:  $0.70 \times [\text{NO}_2]_{\text{Obs.}} + 1.71$ ).

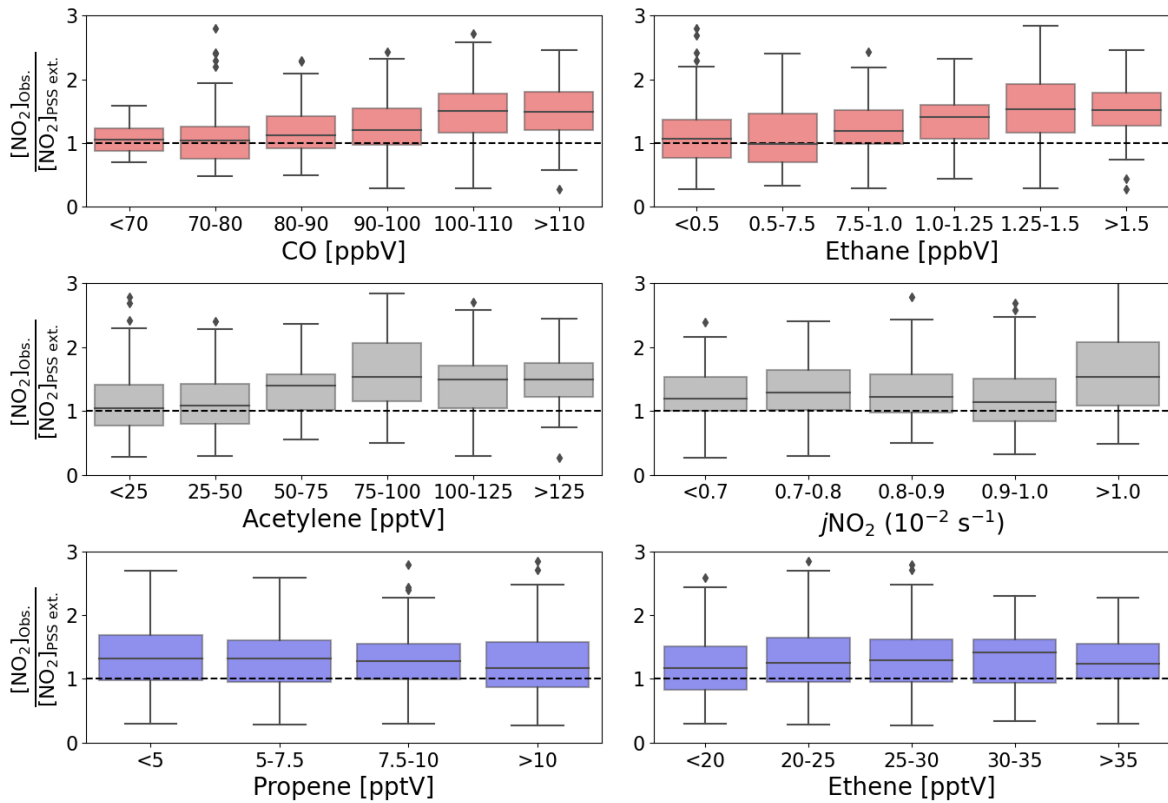


658

659 Figure 4: Monthly plots of midday (12.00-15.00 UTC, local+1) daily averages of  $[\text{NO}_2]_{\text{Obs.}}/[\text{NO}_2]_{\text{PSS ext.}}$  vs. the measured NO mixing ratio. The  
 660 solid lines represent a ratio of 1 between the observed and predicted  $\text{NO}_2$ . The error bars represent  $\pm 2\sigma$  uncertainty on the calculated ratio and  
 661 measured NO. The colours represent the year of the measurements: 2017 = blue, 2018 = red, 2019 = orange, 2020 = grey. The dashed lines  
 662 represent  $([\text{NO}_2]_{\text{PSS ext.}} + 0.957 \text{ pptV})/[\text{NO}_2]_{\text{PSS ext.}}$  to visualise the effect of a  $\text{NO}_2$  artefact of 0.97 pptV on the ratio using the average measured  
 663  $j\text{NO}_2$  and  $\text{O}_3$  and modelled  $\text{HO}_2$  and  $\text{RO}_2$  for each month and the annually average measured IO and BrO for the CVAO. The uncertainty of each

664 data point has been determined from measurement uncertainties in Table 2, the uncertainties in the measured BrO and IO described in the text,  
665 and 20% uncertainty on all the rate coefficients. The uncertainty in the modelled radicals has not been included.

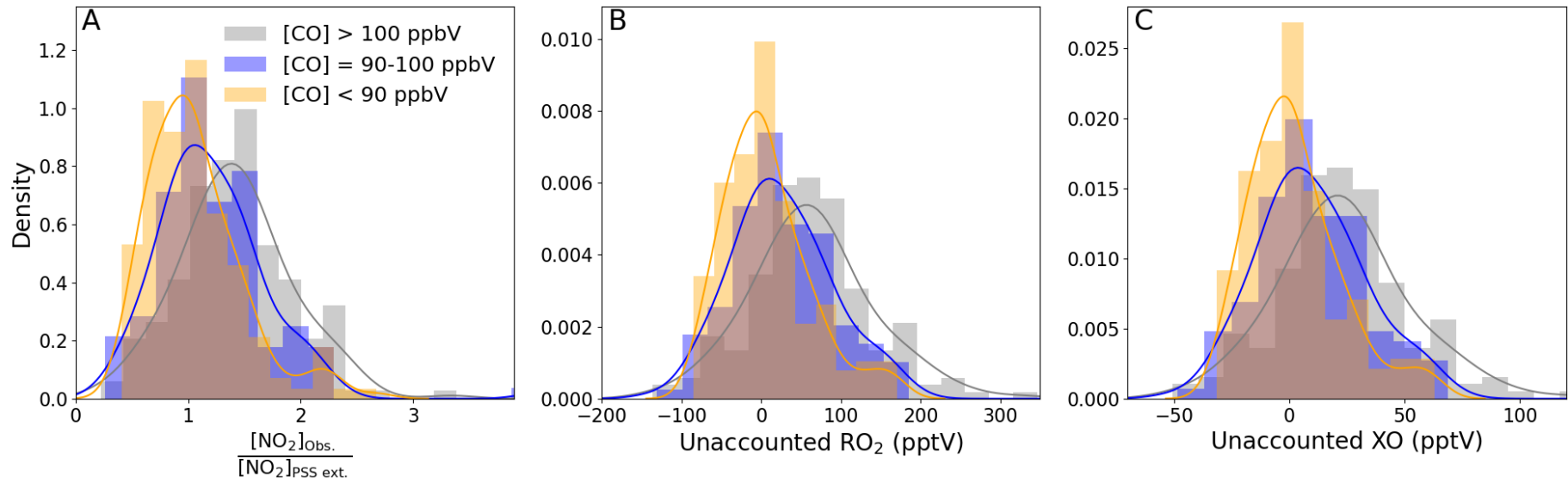
666



667

668 Figure 5: Boxplots of midday (12.00-15.00 UTC, local +1) daily averages of  
 669  $[\text{NO}_2]_{\text{obs.}}/[\text{NO}_2]_{\text{PSS ext.}}$  from July 2017 to June 2020 plotted against intervals of five different  
 670 measured precursors for either  $\text{HO}_2$  or  $\text{RO}_2$  and  $j\text{NO}_2$ . The black dashed lines represent a ratio  
 671 of 1.

672



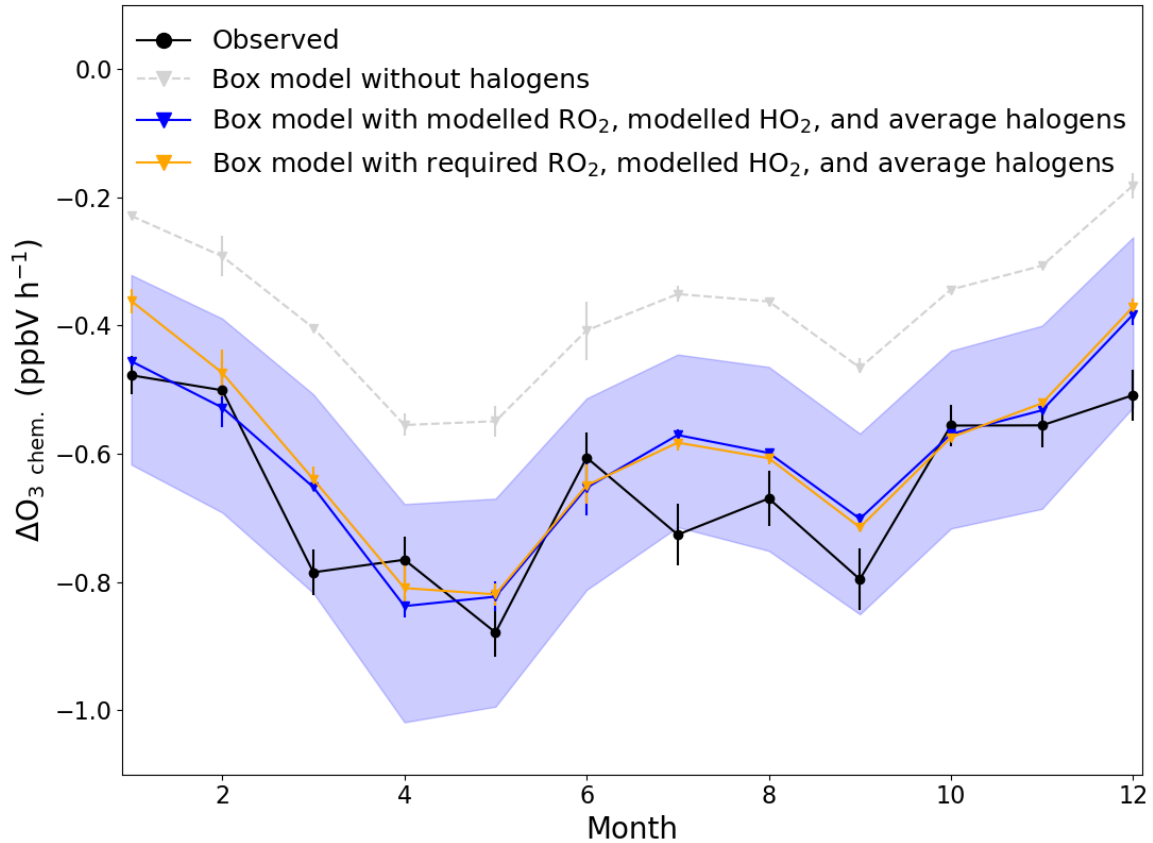
673

674 Figure 6: Density distributions of (A)  $[\text{NO}_2]_{\text{Obs.}}/[\text{NO}_2]_{\text{PSS ext.}}$ , (B) missing  $\text{RO}_2$ , and (C) missing XO separated by measured CO mixing ratios. An  
 675  $\text{NO}_2$  artefact of 0.7 pptV has been subtracted from all data.

676

677





678

679 Figure 7: Average monthly  $\Delta O_3$  due to chemical loss between 09.30 (09.00-10.00) and 17.30  
 680 (17.00-18.00) UTC for each month (black) compared to box modelled  $\Delta O_3$  due to chemical  
 681 loss using modelled  $RO_2$  and  $HO_2$  with (blue) and without (grey) halogen monoxides (BrO and  
 682 IO), and using required  $RO_2$  to get  $[NO_2]_{Obs.}/[NO_2]_{PSS\ ext.} = 1$ , modelled  $HO_2$ , and the annually  
 683 averaged halogen monoxides (orange). The error bars on the observed chemical loss is the  
 684 standard error of all the days used for each month and for the box model it is the minimum and  
 685 maximum  $\Delta O_3$  modelled for each month. The blue shaded area show the possible variability  
 686 in the chemical loss when including the measured halogens at the CVAO (BrO;  $2.5 \pm 1.1$  pptV,  
 687 IO;  $1.4 \pm 0.8$  pptV) (Read et al., 2008).

## 688 10 Tables

689 **Table 1: Summary of previous studies which have compared [RO<sub>x</sub>]<sub>PSS</sub> against measured and/or modelled [RO<sub>x</sub>] in rural, marine and**  
690 **remote conditions.**

Location	NO <sub>x</sub> instrument	NO <sub>x</sub>	$\phi^a$	$\frac{[\text{RO}_x]_{\text{PSS}}}{[\text{RO}_x]_{\text{Measured}}}$ <sup>b</sup>	$\frac{[\text{RO}_x]_{\text{PSS}}}{[\text{RO}_x]_{\text{Model}}}$ <sup>b</sup>	$\frac{[\text{RO}_x]_{\text{Measured}}}{[\text{RO}_x]_{\text{Model}}}$ <sup>b</sup>	Reference
<b>Rural conditions</b>							
Hohenpeissenberg, Germany	CLD with PLC <sup>c</sup>	NO; 50-7000 pptV	2-5.7 <sup>d</sup>	2-3 <sup>e</sup>	-	-	(Mannschreck et al., 2004)
Pearl River Delta, China	CLD with PLC <sup>c</sup>	NO; 50-4000 pptV	1-8.5 <sup>d</sup>	~ 1 <sup>e</sup>	2-10	~ 2 <sup>e</sup>	(Ma et al., 2017)
Pabstthum, Germany	CLD with PLC <sup>c</sup>	1-7 ppbV	1.1-3.0 <sup>d</sup>	~ 4 <sup>e</sup>	-	-	(Volz-Thomas et al., 2003)
Idaho Hill, Colorado	CLD with PLC <sup>c</sup>	38 pptV-21.3 ppbV	-	2.1 (mean) <sup>e</sup>	-	~ 1 <sup>e, f</sup>	(Cantrell et al., 1997; Williams et al., 1997)
Pine forest, Alabama	CLD with PLC <sup>c</sup>	1-5 ppbV	-	1-2 <sup>e</sup>	-	~ 1 <sup>e, f</sup>	(Cantrell et al., 1992; Cantrell et al., 1993a; Parrish et al., 1986)
Essex, England	CLD with Mo <sup>g</sup>	NO; 0.3-9.9 ppbV	-	-	-	~ 1.4 <sup>e</sup>	(Emmerson et al., 2007)
Ponderosa pine forest, Rocky Mountains	CLD with PLC <sup>c</sup>	NO; 100-150 pptV	-	-	-	<3 <sup>h</sup>	(Wolfe et al., 2014)
<b>Marine/Remote with pollution</b>							
Arabian Peninsula	CLD with PLC <sup>c</sup> and CRDS <sup>i</sup>	< 50 pptV - > 10 ppbV	-	-	<u>0.95 (median)</u> ~ 1	-	(Tadic et al., 2020)
Amazon Basin (Manaus)	CLD with PLC <sup>c</sup>	100 pptV - 30 ppbV	1-6 <sup>d</sup>	-	~ 1 <sup>k</sup>	-	(Trebs et al., 2012)
<b>Marine/Remote conditions</b>							
South Atlantic Ocean	CLD with PLC <sup>c</sup>	NO <sub>2</sub> ; 3-20 pptV	1-12.5 <sup>l</sup>	1.27 <sup>e</sup>	~ 5	~ 4 <sup>e</sup>	(Hosaynali Beygi et al., 2011)
Mauna Loa, Hawaii	CLD with PLC <sup>c</sup>	20-60 pptV	1.4-2.2	1.5-3 <sup>e</sup>	2-3.5	1.2-2 <sup>e</sup>	(Hauglustaine et al., 1996)
Mace Head, Ireland	CLD with TC <sup>m</sup>	NO < 10 pptV	-	-	-	~ 0.25 <sup>e</sup>	(Carpenter et al., 1997; Cox, 1999)
Cape Grim, Tasmania	CLD with PLC <sup>c</sup>	NO < 5 pptV	-	-	-	~ 0.4 <sup>e</sup>	(Carpenter et al., 1997; Cox, 1999)
Cabo Verde	CLD with PLC <sup>c</sup>	< 50 pptV	0.45-12.0 <sup>d</sup> (median = 2.1)	-	1.5 (median)	-	This study

691 <sup>a</sup>Without radicals and halogens. <sup>b</sup>[RO<sub>x</sub>] = [HO<sub>2</sub>] + [RO<sub>2</sub>]. <sup>c</sup>CLD with PLC = Detection by chemiluminescence with photolytic converter for NO<sub>2</sub>.  
692 <sup>d</sup>Increasing  $\phi$  with decreasing [NO], [NO<sub>2</sub>] or [NO<sub>x</sub>]. <sup>e</sup>[RO<sub>x</sub>] measured by chemical amplification. <sup>f</sup>Calculated/modelled using steady state theory.  
693 <sup>g</sup>CLD with Mo = Detection by chemiluminescence with molybdenum converter. <sup>h</sup>[RO<sub>x</sub>] measured by Peroxy Radical Chemical Ionization Mass  
694 Spectrometry (PeRCIMS). <sup>i</sup>CRDS = Cavity Ring down spectroscopy. <sup>k</sup>PSS derived [RO<sub>x</sub>] was within the range of the modelled values. <sup>l</sup>Increasing  
695  $\phi$  with increasing [NO<sub>2</sub>]. <sup>m</sup>CLD with TC = Detection by chemiluminescence with thermal converter.

696 **Table 2: Overview of instruments and measurements used from the CVAO.**

Instrument	Measurement	<u>2<math>\sigma</math> Hourly</u> <u>Uncertainty Accuracy</u>	DJF <sup>a</sup>	MAM <sup>a</sup>	JJA <sup>a</sup>	SON <sup>a</sup>	Reference <sup>b</sup>
AQD	NO (pptV)	1.4 pptV <sup>c</sup> ( <u>55 %</u> ) <sup>d</sup>	5.3 $\pm$ 7.8	1.9 $\pm$ 4.2	2.7 $\pm$ 5.6	3.6 $\pm$ 5.9	Andersen et al. (2021)
	NO <sub>2</sub> (pptV)	4.4 pptV <sup>c</sup> ( <u>36 %</u> ) <sup>d</sup>	27.0 $\pm$ 35.8	10.0 $\pm$ 13.5	10.2 $\pm$ 16.8	10.6 $\pm$ 15.7	
Thermo Scientific 49i	O <sub>3</sub> (ppbV)	0.07 ppbV <sup>e</sup> ( <u>&lt; 1 %</u> )	38.9 $\pm$ 8.8	39.2 $\pm$ 12.1	29.9 $\pm$ 11.9	31.2 $\pm$ 11.1	Read et al. (2008)
Ocean Optics QE650000	<i>j</i> NO <sub>2</sub> (10 <sup>-3</sup> s <sup>-1</sup> )	15 %	7.8 $\pm$ 2.7	9.3 $\pm$ 2.2	8.9 $\pm$ 2.5	8.7 $\pm$ 2.4	See supplementary
	<i>j</i> O( <sup>1</sup> D) (10 <sup>-5</sup> s <sup>-1</sup> )	15 %	1.7 $\pm$ 1.2	3.0 $\pm$ 1.3	2.6 $\pm$ 1.2	2.6 $\pm$ 1.2	
Picarro	CO (ppbV)	1.0 ppbV ( <u>&lt; 2 %</u> )	99.0 $\pm$ 20.2	103 $\pm$ 17	80.0 $\pm$ 19.3	84.5 $\pm$ 16.6	Zellweger et al. (2012, 2016)
	CH <sub>4</sub> (ppbV)	0.3 ppbV ( <u>&lt; 0.1 %</u> )	1916 $\pm$ 26	1914 $\pm$ 29	1886 $\pm$ 34	1896 $\pm$ 30	
GC-FID	Ethane (pptV)	5.2 %	1438 $\pm$ 600	1204 $\pm$ 608	518 $\pm$ 267	660 $\pm$ 449	R. Steinbrecher (2019)
	Ethene (pptV)	5.0 %	31.2 $\pm$ 18.6	23.2 $\pm$ 9.8	27.5 $\pm$ 15.1	28.9 $\pm$ 19.6	
	Acetylene (pptV)	10.7 %	134 $\pm$ 86	86.9 $\pm$ 82.4	22.6 $\pm$ 22.2	38.1 $\pm$ 38.5	
	Propane (pptV)	5.6 %	336 $\pm$ 259	148 $\pm$ 195	20.6 $\pm$ 18.7	71.0 $\pm$ 133	
	Propene (pptV)	6.9 %	8.6 $\pm$ 8.6	8.8 $\pm$ 11.5	8.0 $\pm$ 6.2	7.2 $\pm$ 6.1	
	Iso-butane (pptV)	6.4 %	40.4 $\pm$ 39.5	11.0 $\pm$ 20.0	3.2 $\pm$ 4.3	8.4 $\pm$ 15.5	
	n-butane (pptV)	5.0 %	82.8 $\pm$ 80.7	19.4 $\pm$ 36.0	6.0 $\pm$ 7.3	22.1 $\pm$ 40.5	
	Iso-pentane (pptV)	4.6 %	11.1 $\pm$ 14.9	3.6 $\pm$ 6.2	5.2 $\pm$ 9.5	4.0 $\pm$ 6.7	
	n-pentane (pptV)	6.4 %	8.7 $\pm$ 11.4	2.9 $\pm$ 4.7	1.7 $\pm$ 2.6	3.5 $\pm$ 5.2	
	Benzene (pptV)	4.8 %	40.1 $\pm$ 30.5	22.9 $\pm$ 23.3	11.1 $\pm$ 10.5	17.3 $\pm$ 11.5	
	Toluene (pptV)	6.3 %	4.6 $\pm$ 5.4	3.0 $\pm$ 4.2	2.9 $\pm$ 2.8	3.4 $\pm$ 3.1	
	Methanol (pptV)	20.7 %	486 $\pm$ 563	698 $\pm$ 734	677 $\pm$ 603	857 $\pm$ 655	
	Acetone (pptV)	12.2 %	506 $\pm$ 263	614 $\pm$ 274	767 $\pm$ 332	681 $\pm$ 213	
Campbell Scientific weather station	Temperature (°C)	0.4 °C at 5-40 °C	22.0 $\pm$ 2.3	21.7 $\pm$ 1.4	24.5 $\pm$ 2.5	25.8 $\pm$ 2.1	Carpenter et al. (2010)
	Pressure (hPa)	1.0 hPa at 0-40°C	1016 $\pm$ 4	1016 $\pm$ 3	1015 $\pm$ 4	1014 $\pm$ 3	
	Relative Humidity (%)	2 % at 10-90 %	74.9 $\pm$ 12.8	77.2 $\pm$ 10.4	82.8 $\pm$ 8.8	81.1 $\pm$ 11.9	
	Solar Radiation (W m <sup>-2</sup> )	5%	615 $\pm$ 312	785 $\pm$ 251	737 $\pm$ 283	716 $\pm$ 273	

697 <sup>a</sup>Midday (12.00-15.00 UTC, local +1) mean  $\pm 2\sigma$  for July 2017 – June 2020. <sup>b</sup>For further information on the instrument and the data processing.  
 698 <sup>c</sup>Average uncertainties determined as described in Andersen et al. (2021). <sup>d</sup>Percentage given is relevant to average midday uncertainty. <sup>e</sup>Estimated  
 699 from zero measurements and from running two O<sub>3</sub> instruments together.

700

701 **Table 3: Potential sources of NO<sub>2</sub> artefacts at the CVAO.**

	ACS at 380 nm (10 <sup>-20</sup> cm <sup>2</sup> ) <sup>a</sup>	ACS at 385 nm (10 <sup>-20</sup> cm <sup>2</sup> ) <sup>a</sup>	ACS at 390 nm (10 <sup>-20</sup> cm <sup>2</sup> ) <sup>a</sup>	Conversion efficiency (%) <sup>b</sup>	Measured at the CVAO at midday (pptV) <sup>c</sup>	Modelled by GEOS Chem at midday (pptV) <sup>c</sup>	Potential artefact (pptV)
NO <sub>2</sub> $\xrightarrow{hv}$ NO	59.24	59.42	62.0	50	-	-	-
BrONO <sub>2</sub> $\xrightarrow{hv}$ NO <sub>2</sub>	3.85	3.37	2.97	2.8	-	0.5-1.5	0.014-0.042
ClONO <sub>2</sub> $\xrightarrow{hv}$ NO <sub>2</sub>	0.121	0.137	0.091	0.1	-	0.5-1	0.0005-0.001
CINO $\xrightarrow{hv}$ NO	8.86	7.82	6.86	6.6	-	-	-
CINO <sub>2</sub> $\xrightarrow{hv}$ NO <sub>2</sub>	0.3593	0.2687	0.2008	0.2	-	~0	-
BrNO <sub>2</sub> $\xrightarrow{hv}$ NO <sub>2</sub>	17	17	16	14.3	-	~0	-
HONO $\xrightarrow{hv}$ NO	9.2	14.5	2.4	6.3	3-5	0.2-0.4	0.38-0.63
PAN $\xrightarrow{\Delta}$ NO <sub>2</sub>	-	-	-	~5	< 6	~20	< <del>0.283</del>
<b>Total</b>	-	-	-	-	-	-	<b><del>0.679-0.975</del></b>

702 <sup>a</sup>All absorption cross sections have been reported by IUPAC (Atkinson et al., 2004). <sup>b</sup>The reported conversion efficiencies have been calculated  
 703 based on a NO<sub>2</sub> CE of 50%. <sup>c</sup>Midday is defined as 12.00-15.00 UTC (local+1).

704 **Table 4: Summary over the required additional artefact, RO<sub>2</sub>, and XO to give [NO<sub>2</sub>]<sub>Obs.</sub>/[NO<sub>2</sub>]<sub>PSS ext.</sub> = 1 given as 50<sup>th</sup> (25<sup>th</sup>-75<sup>th</sup>) percentile**  
 705 **when subtracting a NO<sub>2</sub> artefact of 0.7 pptV.**

	[CO] < 90 ppbV	90 ppbV < [CO] < 100 ppbV	[CO] > 100 ppbV
$\frac{[\text{NO}_2]_{\text{Obs.}}}{[\text{NO}_2]_{\text{PSS ext.}}}$	1.00 (0.76 - 1.29)	1.14 (0.89 - 1.47)	1.42 (1.12 - 1.68)
Required additional artefact (pptV)	0.00 (-2.65 - 1.70)	1.9 (0.92 - 5.27)	4.4 (0.95 - 9.27)
<b>Case I: Using BrO = 2.5 pptV and IO = 1.4 pptV</b>			
Required RO <sub>x</sub> (pptV) <sup>a</sup>	49.45 (16.18 - 87.63)	65.0 (33.68 - 112.5)	109.7 (63.14 - 149.5)
Modelled RO <sub>x</sub> (pptV)	48.89 (46.01 - 53.35)	45.60 (35.69 - 54.71)	44.99 (37.31 - 54.70)
Required RO <sub>2</sub> (pptV) <sup>b</sup>	31.77 (-1.79 - 69.99)	47.53 (16.81 - 93.93)	90.49 (45.04 - 128.5)
Modelled RO <sub>2</sub> (pptV)	33.66 (30.07 - 34.43)	29.89 (21.50 - 36.32)	27.62 (20.93 - 35.42)
Missing RO <sub>2</sub> (pptV) <sup>c</sup>	-0.25 (-31.85 - 39.69)	20.19 (-14.23 - 66.44)	61.33 (18.53 - 104.3)
<b>Case II: Using modelled RO<sub>2</sub> and HO<sub>2</sub></b>			
Required XO (pptV) <sup>d</sup>	3.72 (-7.94 - 18.55)	11.31 (-1.46 - 28.46)	26.58 (10.70 - 42.52)
Missing XO (pptV) <sup>e</sup>	-0.18 (-11.84 - 14.65)	7.41 (-5.36 - 24.56)	22.68 (6.80 - 38.62)

706 <sup>a</sup>Calculated using equation (IV). <sup>b</sup>Calculated using equation (VIII). <sup>c</sup>Calculated using equation (IX). <sup>d</sup>Calculated using equation (V). <sup>e</sup>Subtracted  
 707 3.9 pptV of XO from the required XO (2.5 pptV BrO + 1.4 pptV IO).

## 11 References

- 710 Andersen, S. T., Carpenter, L. J., Nelson, B. S., Neves, L., Read, K. A., Reed, C., Ward, M.,  
Rowlinson, M. J., and Lee, J. D.: Long-term NO<sub>x</sub> measurements in the remote marine tropical  
troposphere, *Atmos. Meas. Tech.*, 14, 3071-3085, 10.5194/amt-14-3071-2021, 2021.
- Atkinson, R., Baulch, D. L., Cox, R. A., Crowley, J. N., Hampson, R. F., Hynes, R. G., Jenkin,  
M. E., Rossi, M. J., and Troe, J.: IUPAC Task Group on Atmospheric Chemical Kinetic Data  
Evaluation, *Atmos. Chem. Phys.*, 4, 2004.
- 715 Atkinson, R., Baulch, D. L., Cox, R. A., Crowley, J. N., Hampson, R. F., Hynes, R. G., Jenkin,  
M. E., Rossi, M. J., Troe, J., and Subcommittee, I.: Evaluated kinetic and photochemical data  
for atmospheric chemistry: Volume II &ndash; gas phase reactions of organic species, *Atmos.*  
*Chem. Phys.*, 6, 3625-4055, 10.5194/acp-6-3625-2006, 2006.
- Ayers, G. P., Penkett, S. A., Gillett, R. W., Bandy, B., Galbally, I. E., Meyer, C. P., Elsworth,  
720 C. M., Bentley, S. T., and Forgan, B. W.: Evidence for photochemical control of ozone  
concentrations in unpolluted marine air, *Nature*, 360, 446-449, 10.1038/360446a0, 1992.
- Ayers, G. P., and Galbally, I. E.: A preliminary investigation of a boundary layer-free  
troposphere entrainment velocity at Cape Grim, *Baseline* 92, 1995.
- Bloss, W. J., Evans, M. J., Lee, J. D., Sommariva, R., Heard, D. E., and Pilling, M. J.: The  
725 oxidative capacity of the troposphere: Coupling of field measurements of OH and a global  
chemistry transport model, *Faraday Discussions*, 130, 425-436, 10.1039/B419090D, 2005.
- Bradshaw, J., Davis, D., Crawford, J., Chen, G., Shetter, R., Müller, M., Gregory, G., Sachse,  
G., Blake, D., Heikes, B., Singh, H., Mastromarino, J., and Sandholm, S.: Photofragmentation  
two-photon laser-induced fluorescence detection of NO<sub>2</sub> and NO: Comparison of  
730 measurements with model results based on airborne observations during PEM-Tropics A,  
*Geophysical Research Letters*, 26, 471-474, <https://doi.org/10.1029/1999GL900015>, 1999.
- Bridier, I., Caralp, F., Loirat, H., Lesclaux, R., Veyret, B., Becker, K. H., Reimer, A., and  
Zabel, F.: Kinetic and theoretical studies of the reactions acetylperoxy + nitrogen dioxide + M  
.dblarw. acetyl peroxy + M between 248 and 393 K and between 30 and 760 torr, *The*  
735 *Journal of Physical Chemistry*, 95, 3594-3600, 10.1021/j100162a031, 1991.
- Burkert, J., Andrés-Hernández, M.-D., Stöbener, D., Burrows, J. P., Weissenmayer, M., and  
Kraus, A.: Peroxy radical and related trace gas measurements in the boundary layer above the  
Atlantic Ocean, *Journal of Geophysical Research: Atmospheres*, 106, 5457-5477,  
<https://doi.org/10.1029/2000JD900613>, 2001.
- 740 Butkovskaya, N., Kukui, A., and Le Bras, G.: HNO<sub>3</sub> Forming Channel of the HO<sub>2</sub> + NO  
Reaction as a Function of Pressure and Temperature in the Ranges of 72–600 Torr and 223–323  
K, *The Journal of Physical Chemistry A*, 111, 9047-9053, 10.1021/jp074117m, 2007.
- Butkovskaya, N., Rayez, M.-T., Rayez, J.-C., Kukui, A., and Le Bras, G.: Water Vapor Effect  
on the HNO<sub>3</sub> Yield in the HO<sub>2</sub> + NO Reaction: Experimental and Theoretical Evidence, *The*  
745 *Journal of Physical Chemistry A*, 113, 11327-11342, 10.1021/jp811428p, 2009.
- Calvert, J. G., and Stockwell, W. R.: Deviations from the O<sub>3</sub>–NO–NO<sub>2</sub> photostationary state  
in tropospheric chemistry, *Canadian Journal of Chemistry*, 61, 983-992, 10.1139/v83-174,  
1983.
- Cantrell, C. A., Lind, J. A., Shetter, R. E., Calvert, J. G., Goldan, P. D., Kuster, W., Fehsenfeld,  
750 F. C., Montzka, S. A., Parrish, D. D., Williams, E. J., Buhr, M. P., Westberg, H. H., Allwine,  
G., and Martin, R.: Peroxy radicals in the ROSE experiment: Measurement and theory, *Journal*  
*of Geophysical Research: Atmospheres*, 97, 20671-20686, <https://doi.org/10.1029/92JD01727>,  
1992.
- Cantrell, C. A., Shetter, R. E., Calvert, J. G., Parrish, D. D., Fehsenfeld, F. C., Goldan, P. D.,  
755 Kuster, W., Williams, E. J., Westberg, H. H., Allwine, G., and Martin, R.: Peroxy radicals as  
measured in ROSE and estimated from photostationary state deviations, *Journal of*

- Geophysical Research: Atmospheres, 98, 18355-18366, <https://doi.org/10.1029/93JD01794>, 1993a.
- 760 Cantrell, C. A., Shetter, R. E., Lind, J. A., McDaniel, A. H., Calvert, J. G., Parrish, D. D., Fehsenfeld, F. C., Buhr, M. P., and Trainer, M.: An improved chemical amplifier technique for peroxy radical measurements, *Journal of Geophysical Research: Atmospheres*, 98, 2897-2909, <https://doi.org/10.1029/92JD02842>, 1993b.
- 765 Cantrell, C. A., Shetter, R. E., Gilpin, T. M., and Calvert, J. G.: Peroxy radicals measured during Mauna Loa Observatory Photochemistry Experiment 2: The data and first analysis, *Journal of Geophysical Research: Atmospheres*, 101, 14643-14652, <https://doi.org/10.1029/95JD01698>, 1996.
- 770 Cantrell, C. A., Shetter, R. E., Calvert, J. G., Eisele, F. L., Williams, E., Baumann, K., Brune, W. H., Stevens, P. S., and Mather, J. H.: Peroxy radicals from photostationary state deviations and steady state calculations during the Tropospheric OH Photochemistry Experiment at Idaho Hill, Colorado, 1993, *Journal of Geophysical Research: Atmospheres*, 102, 6369-6378, <https://doi.org/10.1029/96JD01703>, 1997.
- 775 Carpenter, L. J., Monks, P. S., Bandy, B. J., Penkett, S. A., Galbally, I. E., and Meyer, C. P.: A study of peroxy radicals and ozone photochemistry at coastal sites in the northern and southern hemispheres, *Journal of Geophysical Research: Atmospheres*, 102, 25417-25427, <https://doi.org/10.1029/97JD02242>, 1997.
- Carpenter, L. J., Clemitshaw, K. C., Burgess, R. A., Penkett, S. A., Cape, J. N., and McFadyen, G. G.: Investigation and evaluation of the NO<sub>x</sub>/O<sub>3</sub> photochemical steady state, *Atmospheric Environment*, 32, 3353-3365, [https://doi.org/10.1016/S1352-2310\(97\)00416-0](https://doi.org/10.1016/S1352-2310(97)00416-0), 1998.
- 780 Carpenter, L. J., Fleming, Z. L., Read, K. A., Lee, J. D., Moller, S. J., Hopkins, J. R., Purvis, R. M., Lewis, A. C., Müller, K., Heinold, B., Herrmann, H., Fomba, K. W., van Pinxteren, D., Müller, C., Tegen, I., Wiedensohler, A., Müller, T., Niedermeier, N., Achterberg, E. P., Patey, M. D., Kozlova, E. A., Heimann, M., Heard, D. E., Plane, J. M. C., Mahajan, A., Oetjen, H., Ingham, T., Stone, D., Whalley, L. K., Evans, M. J., Pilling, M. J., Leigh, R. J., Monks, P. S., Karunaharan, A., Vaughan, S., Arnold, S. R., Tschritter, J., Pöhler, D., Frieß, U., Holla, R.,
- 785 Mendes, L. M., Lopez, H., Faria, B., Manning, A. J., and Wallace, D. W. R.: Seasonal characteristics of tropical marine boundary layer air measured at the Cape Verde Atmospheric Observatory, *Journal of Atmospheric Chemistry*, 67, 87-140, 10.1007/s10874-011-9206-1, 2010.
- 790 Carsey, T. P., Churchill, D. D., Farmer, M. L., Fischer, C. J., Pszenny, A. A., Ross, V. B., Saltzman, E. S., Springer-Young, M., and Bonsang, B.: Nitrogen oxides and ozone production in the North Atlantic marine boundary layer, *Journal of Geophysical Research: Atmospheres*, 102, 10653-10665, 10.1029/96JD03511, 1997.
- 795 Clemitshaw, K. C., Carpenter, L. J., Penkett, S. A., and Jenkin, M. E.: A calibrated peroxy radical chemical amplifier for ground-based tropospheric measurements, *Journal of Geophysical Research: Atmospheres*, 102, 25405-25416, <https://doi.org/10.1029/97JD01902>, 1997.
- Cox, R. A.: Ozone and peroxy radical budgets in the marine boundary layer: Modeling the effect of NO<sub>x</sub>, *Journal of Geophysical Research: Atmospheres*, 104, 8047-8056, <https://doi.org/10.1029/1998JD100104>, 1999.
- 800 Crawford, J., Davis, D., Chen, G., Bradshaw, J., Sandholm, S., Gregory, G., Sachse, G., Anderson, B., Collins, J., Blake, D., Singh, H., Heikes, B., Talbot, R., and Rodriguez, J.: Photostationary state analysis of the NO<sub>2</sub>-NO system based on airborne observations from the western and central North Pacific, *Journal of Geophysical Research: Atmospheres*, 101, 2053-2072, <https://doi.org/10.1029/95JD02201>, 1996.



- 805 Duncianu, M., Lahib, A., Tomas, A., Stevens, P. S., and Dusanter, S.: Characterization of a chemical amplifier for peroxy radical measurements in the atmosphere, *Atmospheric Environment*, 222, 117106, <https://doi.org/10.1016/j.atmosenv.2019.117106>, 2020.
- Emmerson, K. M., Carslaw, N., Carslaw, D. C., Lee, J. D., McFiggans, G., Bloss, W. J., Gravestock, T., Heard, D. E., Hopkins, J., Ingham, T., Pilling, M. J., Smith, S. C., Jacob, M.,  
810 and Monks, P. S.: Free radical modelling studies during the UK TORCH Campaign in Summer 2003, *Atmos. Chem. Phys.*, 7, 167-181, 10.5194/acp-7-167-2007, 2007.
- Fairlie, T. D., Jacob, D. J., Dibb, J. E., Alexander, B., Avery, M. A., van Donkelaar, A., and Zhang, L.: Impact of mineral dust on nitrate, sulfate, and ozone in transpacific Asian pollution plumes, *Atmos. Chem. Phys.*, 10, 3999-4012, 10.5194/acp-10-3999-2010, 2010.
- 815 Gao, R. S., Keim, E. R., Woodbridge, E. L., Ciciora, S. J., Proffitt, M. H., Thompson, T. L., Mclaughlin, R. J., and Fahey, D. W.: New photolysis system for NO<sub>2</sub> measurements in the lower stratosphere, *Journal of Geophysical Research: Atmospheres*, 99, 20673-20681, <https://doi.org/10.1029/94JD01521>, 1994.
- Handisides, G. M., Plass-Dülmer, C., Gilge, S., Bingemer, H., and Berresheim, H.:  
820 Hohenpeissenberg Photochemical Experiment (HOPE 2000): Measurements and photostationary state calculations of OH and peroxy radicals, *Atmos. Chem. Phys.*, 3, 1565-1588, 10.5194/acp-3-1565-2003, 2003.
- Hauglustaine, D. A., Madronich, S., Ridley, B. A., Walega, J. G., Cantrell, C. A., Shetter, R. E., and Hübler, G.: Observed and model-calculated photostationary state at Mauna Loa  
825 Observatory during MLOPEX 2, *Journal of Geophysical Research: Atmospheres*, 101, 14681-14696, <https://doi.org/10.1029/95JD03612>, 1996.
- Hauglustaine, D. A., Madronich, S., Ridley, B. A., Flocke, S. J., Cantrell, C. A., Eisele, F. L., Shetter, R. E., Tanner, D. J., Ginoux, P., and Atlas, E. L.: Photochemistry and budget of ozone during the Mauna Loa Observatory Photochemistry Experiment (MLOPEX 2), *Journal of  
830 Geophysical Research: Atmospheres*, 104, 30275-30307, <https://doi.org/10.1029/1999JD900441>, 1999.
- Hernández, M. D. A., Burkert, J., Reichert, L., Stöbener, D., Meyer-Arneke, J., Burrows, J. P., Dickerson, R. R., and Doddridge, B. G.: Marine boundary layer peroxy radical chemistry during the AEROSOLS99 campaign: Measurements and analysis, *Journal of Geophysical  
835 Research: Atmospheres*, 106, 20833-20846, <https://doi.org/10.1029/2001JD900113>, 2001.
- Hosaynali Beygi, Z., Fischer, H., Harder, H. D., Martinez, M., Sander, R., Williams, J., Brookes, D. M., Monks, P. S., and Lelieveld, J.: Oxidation photochemistry in the Southern Atlantic boundary layer: unexpected deviations of photochemical steady state, *Atmos. Chem. Phys.*, 11, 8497-8513, 10.5194/acp-11-8497-2011, 2011.
- 840 Inamdar, S., Tinel, L., Chance, R., Carpenter, L. J., Sabu, P., Chacko, R., Tripathy, S. C., Kerkar, A. U., Sinha, A. K., Bhaskar, P. V., Sarkar, A., Roy, R., Sherwen, T., Cuevas, C., Saiz-Lopez, A., Ram, K., and Mahajan, A. S.: Estimation of reactive inorganic iodine fluxes in the Indian and Southern Ocean marine boundary layer, *Atmos. Chem. Phys.*, 20, 12093-12114, 10.5194/acp-20-12093-2020, 2020.
- 845 Jacob, D. J., Heikes, E. G., Fan, S.-M., Logan, J. A., Mauzerall, D. L., Bradshaw, J. D., Singh, H. B., Gregory, G. L., Talbot, R. W., Blake, D. R., and Sachse, G. W.: Origin of ozone and NO<sub>x</sub> in the tropical troposphere: A photochemical analysis of aircraft observations over the South Atlantic basin, 101, 24235-24250, doi:10.1029/96JD00336, 1996.
- Jenkin, M. E., Young, J. C., and Rickard, A. R.: The MCM v3.3.1 degradation scheme for isoprene, *Atmos. Chem. Phys.*, 15, 11433-11459, 10.5194/acp-15-11433-2015, 2015.
- 850 Kleindienst, T. E.: Recent developments in the chemistry and biology of peroxyacetyl nitrate, *Research on Chemical Intermediates*, 20, 335-384, 10.1163/156856794X00379, 1994.
- Lee, J. D., Moller, S. J., Read, K. A., Lewis, A. C., Mendes, L., and Carpenter, L. J.: Year-round measurements of nitrogen oxides and ozone in the tropical North Atlantic marine

- 855 boundary layer, *Journal of Geophysical Research: Atmospheres*, 114,  
<https://doi.org/10.1029/2009JD011878>, 2009.
- Leighton, P. A.: *Photochemistry of Air Pollution*, Academic Press, 1961.
- Liu, Y., and Zhang, J.: Atmospheric Peroxy Radical Measurements Using Dual-Channel  
Chemical Amplification Cavity Ringdown Spectroscopy, *Analytical chemistry*, 86, 5391-5398,  
860 10.1021/ac5004689, 2014.
- Ma, Y., Lu, K., Chou, C. C. K., Li, X., and Zhang, Y.: Strong deviations from the NO-NO<sub>2</sub>-  
O<sub>3</sub> photostationary state in the Pearl River Delta: Indications of active peroxy radical and  
chlorine radical chemistry, *Atmospheric Environment*, 163, 22-34,  
<https://doi.org/10.1016/j.atmosenv.2017.05.012>, 2017.
- 865 Mahajan, A. S., Plane, J. M. C., Oetjen, H., Mendes, L., Saunders, R. W., Saiz-Lopez, A.,  
Jones, C. E., Carpenter, L. J., and McFiggans, G. B.: Measurement and modelling of  
tropospheric reactive halogen species over the tropical Atlantic Ocean, *Atmos. Chem. Phys.*,  
10, 4611-4624, 10.5194/acp-10-4611-2010, 2010.
- Mahajan, A. S., Whalley, L. K., Kozlova, E., Oetjen, H., Mendez, L., Furneaux, K. L.,  
870 Goddard, A., Heard, D. E., Plane, J. M. C., and Saiz-Lopez, A.: DOAS observations of  
formaldehyde and its impact on the HO<sub>x</sub> balance in the tropical Atlantic marine boundary layer,  
*Journal of Atmospheric Chemistry*, 66, 167, 10.1007/s10874-011-9200-7, 2011.
- Manschreck, K., Gilge, S., Plass-Duelmer, C., Fricke, W., and Berresheim, H.: Assessment  
of the applicability of NO-NO<sub>2</sub>-O<sub>3</sub> photostationary state to long-  
875 term measurements at the Hohenpeissenberg GAW Station, Germany, *Atmos. Chem. Phys.*, 4,  
1265-1277, 10.5194/acp-4-1265-2004, 2004.
- Mihele, C. M., and Hastie, D. R.: The sensitivity of the radical amplifier to ambient water  
vapour, *Geophysical Research Letters*, 25, 1911-1913, <https://doi.org/10.1029/98GL01432>,  
1998.
- 880 Miyazaki, K., Parker, A. E., Fittschen, C., Monks, P. S., and Kajii, Y.: A new technique for the  
selective measurement of atmospheric peroxy radical concentrations of HO<sub>2</sub> and  
RO<sub>2</sub> using a denuding method, *Atmos. Meas. Tech.*, 3, 1547-1554, 10.5194/amt-  
3-1547-2010, 2010.
- Parrish, D. D., Trainer, M., Williams, E. J., Fahey, D. W., Hübler, G., Eubank, C. S., Liu, S.  
885 C., Murphy, P. C., Albritton, D. L., and Fehsenfeld, F. C.: Measurements of the NO<sub>x</sub>-O<sub>3</sub>  
photostationary state at Niwot Ridge, Colorado, *Journal of Geophysical Research:*  
*Atmospheres*, 91, 5361-5370, <https://doi.org/10.1029/JD091iD05p05361>, 1986.
- Parrish, D. D., Hahn, C. H., Fahey, D. W., Williams, E. J., Bollinger, M. J., Hübler, G., Buhr,  
M. P., Murphy, P. C., Trainer, M., Hsie, E. Y., Liu, S. C., and Fehsenfeld, F. C.: Systematic  
890 variations in the concentration of NO<sub>x</sub> (NO Plus NO<sub>2</sub>) at Niwot Ridge, Colorado, *Journal of*  
*Geophysical Research: Atmospheres*, 95, 1817-1836,  
<https://doi.org/10.1029/JD095iD02p01817>, 1990.
- Peterson, M. C., and Honrath, R. E.: NO<sub>x</sub> and NO<sub>y</sub> over the northwestern North Atlantic:  
Measurements and measurement accuracy, *Journal of Geophysical Research: Atmospheres*,  
895 104, 11695-11707, 1999.
- Pinto, J. P., Dibb, J., Lee, B. H., Rappenglück, B., Wood, E. C., Levy, M., Zhang, R.-Y., Lefer,  
B., Ren, X.-R., Stutz, J., Tsai, C., Ackermann, L., Golovko, J., Herndon, S. C., Oakes, M.,  
Meng, Q.-Y., Munger, J. W., Zahniser, M., and Zheng, J.: Intercomparison of field  
measurements of nitrous acid (HONO) during the SHARP campaign, *Journal of Geophysical*  
900 *Research: Atmospheres*, 119, 5583-5601, <https://doi.org/10.1002/2013JD020287>, 2014.
- Pollack, I. B., Lerner, B. M., and Ryerson, T. B.: Evaluation of ultraviolet light-emitting diodes  
for detection of atmospheric NO<sub>2</sub> by photolysis - chemiluminescence, *Journal of Atmospheric*  
*Chemistry*, 65, 111-125, 10.1007/s10874-011-9184-3, 2010.

- 905 Prados-Roman, C., Cuevas, C. A., Hay, T., Fernandez, R. P., Mahajan, A. S., Royer, S. J., Galí, M., Simó, R., Dachs, J., Großmann, K., Kinnison, D. E., Lamarque, J. F., and Saiz-Lopez, A.: Iodine oxide in the global marine boundary layer, *Atmos. Chem. Phys.*, 15, 583-593, 10.5194/acp-15-583-2015, 2015.
- 910 Read, K. A., Mahajan, A. S., Carpenter, L. J., Evans, M. J., Faria, B. V. E., Heard, D. E., Hopkins, J. R., Lee, J. D., Moller, S. J., Lewis, A. C., Mendes, L., McQuaid, J. B., Oetjen, H., Saiz-Lopez, A., Pilling, M. J., and Plane, J. M. C.: Extensive halogen-mediated ozone destruction over the tropical Atlantic Ocean, *Nature*, 453, 1232, 10.1038/nature07035  
<https://www.nature.com/articles/nature07035#supplementary-information>, 2008.
- 915 Read, K. A., Lee, J. D., Lewis, A. C., Moller, S. J., Mendes, L., and Carpenter, L. J.: Intra-annual cycles of NMVOC in the tropical marine boundary layer and their use for interpreting seasonal variability in CO, *Journal of Geophysical Research: Atmospheres*, 114, <https://doi.org/10.1029/2009JD011879>, 2009.
- Reed, C., Evans, M. J., Carlo, P. D., Lee, J. D., and Carpenter, L. J.: Interferences in photolytic NO<sub>2</sub> measurements: explanation for an apparent missing oxidant?, *Atmospheric Chemistry Physics*, 16, 4707-4724, 2016.
- 920 Reed, C., Evans, M. J., Crilley, L. R., Bloss, W. J., Sherwen, T., Read, K. A., Lee, J. D., and Carpenter, L. J.: Evidence for renoxification in the tropical marine boundary layer, *Atmos. Chem. Phys.*, 17, 4081-4092, 10.5194/acp-17-4081-2017, 2017.
- 925 Rhoads, K. P., Kelley, P., Dickerson, R. R., Carsey, T. P., Farmer, M., Savoie, D. L., and Prospero, J. M.: Composition of the troposphere over the Indian Ocean during the monsoonal transition, *Journal of Geophysical Research: Atmospheres*, 102, 18981-18995, 10.1029/97JD01078, 1997.
- Ridley, B. A., Carroll, M. A., Gregory, G. L., and Sachse, G. W.: NO and NO<sub>2</sub> in the troposphere: Technique and measurements in regions of a folded tropopause, *Journal of Geophysical Research: Atmospheres*, 93, 15813-15830, <https://doi.org/10.1029/JD093iD12p15813>, 1988.
- 930 Ridley, B. A., Madronich, S., Chatfield, R. B., Walega, J. G., Shetter, R. E., Carroll, M. A., and Montzka, D. D.: Measurements and model simulations of the photostationary state during the Mauna Loa Observatory Photochemistry Experiment: Implications for radical concentrations and ozone production and loss rates, *Journal of Geophysical Research: Atmospheres*, 97, 10375-10388, <https://doi.org/10.1029/91JD02287>, 1992.
- 935 Ryerson, T. B., Williams, E. J., and Fehsenfeld, F. C.: An efficient photolysis system for fast-response NO<sub>2</sub> measurements, *Journal of Geophysical Research: Atmospheres*, 105, 26447-26461, 10.1029/2000jd900389, 2000.
- 940 Sadanaga, Y., Matsumoto, J., Sakurai, K.-i., Isozaki, R., Kato, S., Nomaguchi, T., Bandow, H., and Kajii, Y.: Development of a measurement system of peroxy radicals using a chemical amplification/laser-induced fluorescence technique, *Review of Scientific Instruments*, 75, 864-872, 10.1063/1.1666985, 2004.
- 945 Saiz-Lopez, A., Plane, J. M. C., Baker, A. R., Carpenter, L. J., von Glasow, R., Gómez Martín, J. C., McFiggans, G., and Saunders, R. W.: Atmospheric Chemistry of Iodine, *Chemical Reviews*, 112, 1773-1804, 10.1021/cr200029u, 2012.
- Sherwen, T., Evans, M. J., Carpenter, L. J., Andrews, S. J., Lidster, R. T., Dix, B., Koenig, T. K., Sinreich, R., Ortega, I., Volkamer, R., Saiz-Lopez, A., Prados-Roman, C., Mahajan, A. S., and Ordóñez, C.: Iodine's impact on tropospheric oxidants: a global model study in GEOS-Chem, *Atmos. Chem. Phys.*, 16, 1161-1186, 10.5194/acp-16-1161-2016, 2016.
- 950 Sillman, S.: The relation between ozone, NO<sub>x</sub> and hydrocarbons in urban and polluted rural environments, *Atmospheric Environment*, 33, 1821-1845, [https://doi.org/10.1016/S1352-2310\(98\)00345-8](https://doi.org/10.1016/S1352-2310(98)00345-8), 1999.

- Sommariva, R., Cox, S., Martin, C., Borońska, K., Young, J., Jimack, P. K., Pilling, M. J., Matthaios, V. N., Nelson, B. S., Newland, M. J., Panagi, M., Bloss, W. J., Monks, P. S., and Rickard, A. R.: AtChem (version 1), an open-source box model for the Master Chemical Mechanism, *Geosci. Model Dev.*, 13, 169-183, 10.5194/gmd-13-169-2020, 2020.
- Steinbrecher, R.: SYSTEM AND PERFORMANCE AUDIT FOR NON METHANE VOLATILE ORGANIC COMPOUNDS: Global GAW Station – Cape Verde Atmospheric Observatory Calhau, Cape Verde, WMO World Calibration Centre for VOC, Karlsruhe Institute of Technology, KIT/IMK-IFU, Garmisch-Partenkirchen, Germany, 2019.
- Syomin, D. A., and Finlayson-Pitts, B. J.: HONO decomposition on borosilicate glass surfaces: implications for environmental chamber studies and field experiments, *Physical Chemistry Chemical Physics*, 5, 5236-5242, 10.1039/B309851F, 2003.
- Tadic, I., Crowley, J. N., Dienhart, D., Eger, P., Harder, H., Hottmann, B., Martinez, M., Parchatka, U., Paris, J. D., Pozzer, A., Rohloff, R., Schuladen, J., Shenolikar, J., Tauer, S., Lelieveld, J., and Fischer, H.: Net ozone production and its relationship to nitrogen oxides and volatile organic compounds in the marine boundary layer around the Arabian Peninsula, *Atmos. Chem. Phys.*, 20, 6769-6787, 10.5194/acp-20-6769-2020, 2020.
- Trebs, I., Mayol-Bracero, O. L., Pauliquevis, T., Kuhn, U., Sander, R., Ganzeveld, L., Meixner, F. X., Kesselmeier, J., Artaxo, P., and Andreae, M. O.: Impact of the Manaus urban plume on trace gas mixing ratios near the surface in the Amazon Basin: Implications for the NO-NO<sub>2</sub>-O<sub>3</sub> photostationary state and peroxy radical levels, *Journal of Geophysical Research: Atmospheres*, 117, <https://doi.org/10.1029/2011JD016386>, 2012.
- Vaughan, S., Ingham, T., Whalley, L. K., Stone, D., Evans, M. J., Read, K. A., Lee, J. D., Moller, S. J., Carpenter, L. J., Lewis, A. C., Fleming, Z. L., and Heard, D. E.: Seasonal observations of OH and HO<sub>2</sub> in the remote tropical marine boundary layer, *Atmos. Chem. Phys.*, 12, 2149-2172, 10.5194/acp-12-2149-2012, 2012.
- Vogt, R., Sander, R., von Glasow, R., and Crutzen, P. J.: Iodine Chemistry and its Role in Halogen Activation and Ozone Loss in the Marine Boundary Layer: A Model Study, *Journal of Atmospheric Chemistry*, 32, 375-395, 10.1023/A:1006179901037, 1999.
- Volz-Thomas, A., Pätz, H.-W., Houben, N., Konrad, S., Mihelcic, D., Klüpfel, T., and Perner, D.: Inorganic trace gases and peroxy radicals during BERLIOZ at Pabstthum: An investigation of the photostationary state of NO<sub>x</sub> and O<sub>3</sub>, *Journal of Geophysical Research: Atmospheres*, 108, PHO 4-1-PHO 4-15, <https://doi.org/10.1029/2001JD001255>, 2003.
- Wang, X., Jacob, D. J., Downs, W., Zhai, S., Zhu, L., Shah, V., Holmes, C. D., Sherwen, T., Alexander, B., Evans, M. J., Eastham, S. D., Neuman, J. A., Veres, P. R., Koenig, T. K., Volkamer, R., Huey, L. G., Bannan, T. J., Percival, C. J., Lee, B. H., and Thornton, J. A.: Global tropospheric halogen (Cl, Br, I) chemistry and its impact on oxidants, *Atmos. Chem. Phys.*, 21, 13973-13996, 10.5194/acp-21-13973-2021, 2021.
- Whalley, L. K., Lewis, A. C., McQuaid, J. B., Purvis, R. M., Lee, J. D., Stemmler, K., Zellweger, C., and Ridgeon, P.: Two high-speed, portable GC systems designed for the measurement of non-methane hydrocarbons and PAN: Results from the Jungfraujoch High Altitude Observatory, *Journal of Environmental Monitoring*, 6, 234-241, 10.1039/B310022G, 2004.
- Whalley, L. K., Furneaux, K. L., Goddard, A., Lee, J. D., Mahajan, A., Oetjen, H., Read, K. A., Kaaden, N., Carpenter, L. J., Lewis, A. C., Plane, J. M. C., Saltzman, E. S., Wiedensohler, A., and Heard, D. E.: The chemistry of OH and HO<sub>2</sub> radicals in the boundary layer over the tropical Atlantic Ocean, *Atmos. Chem. Phys.*, 10, 1555-1576, 10.5194/acp-10-1555-2010, 2010.
- Williams, E. J., Roberts, J. M., Baumann, K., Bertman, S. B., Buhr, S., Norton, R. B., and Fehsenfeld, F. C.: Variations in NO<sub>y</sub> composition at Idaho Hill, Colorado, *Journal of*

- Geophysical Research: Atmospheres, 102, 6297-6314, <https://doi.org/10.1029/96JD03252>, 1997.
- 1005 Wofsy, S. C., Afshar, S., Allen, H. M., Apel, E. C., Asher, E. C., Barletta, B., Bent, J., Bian, H., Biggs, B. C., Blake, D. R., Blake, N., Bourgeois, I., Brock, C. A., Brune, W. H., Budney, J. W., Bui, T. P., Butler, A., Campuzano-Jost, P., Chang, C. S., Chin, M., Commane, R., Correa, G., Crouse, J. D., Cullis, P. D., Daube, B. C., Day, D. A., Dean-Day, J. M., Dibb, J. E., DiGangi, J. P., Diskin, G. S., Dollner, M., Elkins, J. W., Erdesz, F., Fiore, A. M., Flynn, C. M., Froyd, K. D., Gesler, D. W., Hall, S. R., Hanisco, T. F., Hannun, R. A., Hills, A. J., Hintsa, E.
- 1010 J., Hoffman, A., Hornbrook, R. S., Huey, L. G., Hughes, S., Jimenez, J. L., Johnson, B. J., Katich, J. M., Keeling, R. F., Kim, M. J., Kupc, A., Lait, L. R., McKain, K., McLaughlin, R. J., Meinardi, S., Miller, D. O., Montzka, S. A., Moore, F. L., Morgan, E. J., Murphy, D. M., Murray, L. T., Nault, B. A., Neuman, J. A., Newman, P. A., Nicely, J. M., Pan, X., Paplawsky, W., Peischl, J., Prather, M. J., Price, D. J., Ray, E. A., Reeves, J. M., Richardson, M., Rollins,
- 1015 A. W., Rosenlof, K. H., Ryerson, T. B., Scheuer, E., Schill, G. P., Schroder, J. C., Schwarz, J. P., St.Clair, J. M., Steenrod, S. D., Stephens, B. B., Strode, S. A., Sweeney, C., Tanner, D., Teng, A. P., Thames, A. B., Thompson, C. R., Ullmann, K., Veres, P. R., Wagner, N. L., Watt, A., Weber, R., Weinzierl, B. B., Wennberg, P. O., Williamson, C. J., Wilson, J. C., Wolfe, G. M., Woods, C. T., Zeng, L. H., and Vieznor, N.: ATom: Merged Atmospheric Chemistry, Trace
- 1020 Gases, and Aerosols, Version 2, in, ORNL Distributed Active Archive Center, 2021.
- Wolfe, G. M., Cantrell, C., Kim, S., Mauldin Iii, R. L., Karl, T., Harley, P., Turnipseed, A., Zheng, W., Flocke, F., Apel, E. C., Hornbrook, R. S., Hall, S. R., Ullmann, K., Henry, S. B., DiGangi, J. P., Boyle, E. S., Kaser, L., Schnitzhofer, R., Hansel, A., Graus, M., Nakashima, Y., Kajii, Y., Guenther, A., and Keutsch, F. N.: Missing peroxy radical sources within a
- 1025 summertime ponderosa pine forest, *Atmos. Chem. Phys.*, 14, 4715-4732, 10.5194/acp-14-4715-2014, 2014.
- Wood, E. C., and Charest, J. R.: Chemical Amplification - Cavity Attenuated Phase Shift Spectroscopy Measurements of Atmospheric Peroxy Radicals, *Analytical chemistry*, 86, 10266-10273, 10.1021/ac502451m, 2014.
- 1030 Yang, M., Beale, R., Liss, P., Johnson, M., Blomquist, B., and Nightingale, P.: Air-sea fluxes of oxygenated volatile organic compounds across the Atlantic Ocean, *Atmos. Chem. Phys.*, 14, 7499-7517, 10.5194/acp-14-7499-2014, 2014.
- Zellweger, C., Steinbacher, M., and Buchmann, B.: Evaluation of new laser spectrometer techniques for in-situ carbon monoxide measurements, *Atmos. Meas. Tech.*, 5, 2555-2567, 10.5194/amt-5-2555-2012, 2012.
- 1035 Zellweger, C., Emmenegger, L., Firdaus, M., Hatakka, J., Heimann, M., Kozlova, E., Spain, T. G., Steinbacher, M., van der Schoot, M. V., and Buchmann, B.: Assessment of recent advances in measurement techniques for atmospheric carbon dioxide and methane observations, *Atmos. Meas. Tech.*, 9, 4737-4757, 10.5194/amt-9-4737-2016, 2016.
- 1040